MIMO Systems: Principles, Iterative Techniques, and advanced Polarization

Kosai Raoof, Mohammad-Ali Khalighi, Nuttapol Prayongpun

MIMO Systems: Principles, iterative techniques and advanced polarization

K. Raoof [1], M.A. Khalighi [2], and N. Prayongpun [1]

[1]GIPSA-Lab, Département Images et Signal (DIS)
ENSIEG, Domaine Universitaire,
961 rue de Houille Blanche - BP 46
38402 Saint Martin d'Hères cedex
E-mail: kosai.raoof@lis.inpg.fr
Tel: +(33)4 76 82 62 67

[2]Institut Fresnel, UMR CNRS 6133, Marseille, France

15th May 2007

Contents

Chapter 1

1.1 Introduction

This chapter considers the principles of multiple-input multiple-output (MIMO) wireless communication systems as well as some recent accomplishments concerning their implementation. By employing multiple antennas at both transmitter and receiver, very high data rates can be achieved under the condition of deployment in a rich-scattering propagation medium. This interesting property of MIMO systems suggests their use in the future high-rate and high-quality wireless communication systems. Several concepts in MIMO systems are reviewed in this chapter. We first consider "MIMO channel models" and recall the basic principles of MIMO structures and channel modelling. We next study the "MIMO channel capacity" and present the early developments in these systems, concerning the information theory aspect. "Iterative signal detection" is considered next, where we particularly consider iterative techniques for signal detection or in other words, for space-time decoding. As the capacity is inversely proportional to spatial channel correlation, MIMO antennas should be enough separated by several wavelengths. In order to minimize antennas' deploying, we then present the "Advanced polarization diversity techniques for MIMO systems" and explain how these techniques can help us to reduce the spatial correlation in order to achieve high transmission rates. We end the chapter by considering the application of MIMO systems in local area networks, as well as their potential in enhancing range, localisation, and power efficiency of sensor networks.

1.2 MIMO Systems and Channel Models

In this section, a briefly discussed structure based on MIMO communication system is provided. The definition of MIMO channel is described with some related characteristics of wireless communication channels. Recent MIMO channel models are also reported.

1.2.1 MIMO Communication Systems

Using multiple antennas [1] at both transmitter and receiver is to increase the data rate by creating multiple spatial channels. Multiple receiving antennas can also be used to combat fading without expanding the bandwidth of the transmitted signal. In particular, with M_T transmitting and M_R receiving antennas, it is possible to achieve an M-time capacity of single transmitting and single receiving antenna configuration where $M = \min\{M_T, M_R\}$. Fig.1.1 demonstrates a general system employing multiple transmitting and multiple receiving antennas to increase the data rate. A sequence of input symbols is encoded by a space-time encoding function into $M_T \times 1$ discrete-time complex baseband sequence $x[n]$(n is a discrete time index). The $x[n]$ sequence is subsequently transformed by pulse shaping filter into $M_T \times 1$ continuous-time complex baseband sequence $x(t)$ and then the baseband signal is modulated with a transmission carrier. The transmission channel $\mathbf{H}$ superposes the transmitted signal due to the distortions of environment. At the reception side, under the assumption of synchronous sampling, the received signal $y(t)$ with additive noise is down-converted to baseband and sampled to produce a discrete-time signal sequence. Finally, the estimated symbols are decoded by the space time decoding block.

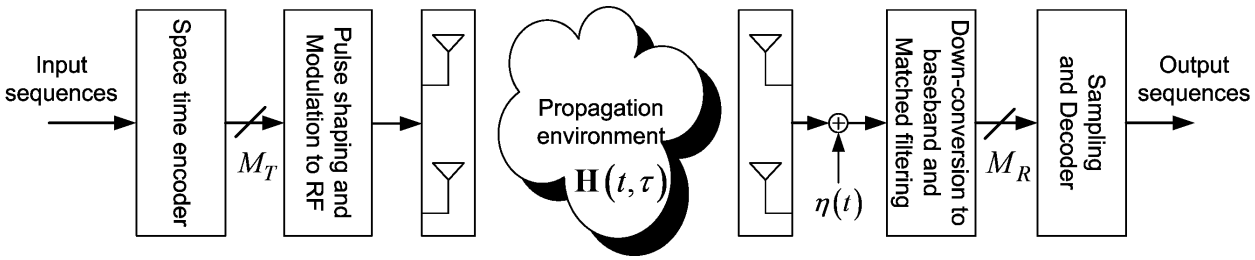

Figure 1.1: General configuration of a MIMO communication system

If the channel is time-invariant, the equivalent received signal at the receiving antenna with M_T elements at the transmitter and M_R elements at the receiver can be written as

$$\mathbf{y}(t) = \sum_{l=0}^{L-1} \mathbf{H}_l \mathbf{x}(t - \tau_l) + \eta(t) \tag{1.1}$$

If the channel is time-variant, the overall MIMO relation can be formulated as

$$\mathbf{y}(t) = \int_{\tau} \mathbf{H}(t, \tau)\mathbf{x}(t - \tau) + \eta(t) \tag{1.2}$$

where $\mathbf{x}(t)$ and $\mathbf{y}(t)$ represent the transmitted and received signals

$$\mathbf{x}(t) = [x_1(t), x_2(t), \ldots, x_{M_T}(t)] \tag{1.3}$$

$$\mathbf{y}(t) = [y_1(t), y_2(t), \ldots, y_{M_R}(t)] \tag{1.4}$$

and L denotes the number of resolvable multipath, τ is the propagation delay, $\mathbf{H}$ is the $M_R \times M_T$ channel matrix at instant τ and finally $\eta(t)$ is an additive noise.

1.2.2 MIMO Channel stationary definition

In wireless communication, stochastic time-variant linear channel usually employs wide sense stationary uncorrelated scattering (WSSUS) for stationary property [2], [3]. This WSSUS channel expresses uncorrelated attenuation in both time-delay and Doppler-shift domains.

The quasi-WSSUS channel [2] is usually applied to real radio systems. It has the properties of a WSSUS channel for a limited bandwidth and for limited time or within a limited environment. This kind of assumption is exceptionally useful in communication systems. For example, Ergodic MIMO channel performance can be given by averaging the channel performances over many independent channel realizations considering that they have the same statistics.

Since in many practical communication systems, the WSSUS property is not truly satisfied

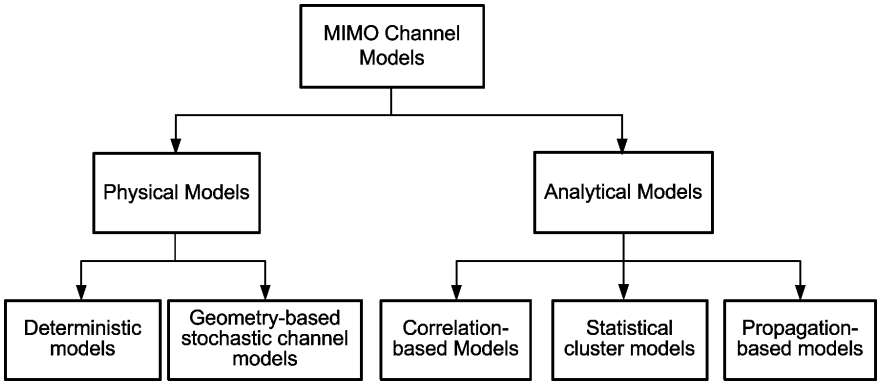

Figure 1.2: MIMO channel and propagation models

because of path loss, shadowing, and varying propagation channel effects. That is why these effects cause the channel to be non-stationary. Non-WSSUS considers also the reflection of the same physical object or/and delay-Doppler dispersion by band or time-limitations at both transmitter and receiver [4].

1.2.3 Classification of MIMO channel modeling

Many different Multiple-input multiple-output channel models have been proposed in the last years. MIMO channel models can be classified as physical and analytical models as shown in Fig.1.2. On the one hand, physical channel models focus on the characteristics of an environment and the electromagnetic wave propagation between the transmitter and the receiver, also they consider the antenna configurations at both ends. On the other hand, analytical models do not provide the site-specific descriptions so that they do not take into account the wave propagation characteristics. The model impulse response is mathematically generated and related to the statistical properties of the propagation environment. However, due to its simplicity, an analytical channel model is very useful for producing MIMO channel matrix for different kind of communication systems.

In literature, physical models can be distinguished into deterministic models [5]-[8] and geometry-based stochastic channel models [9]-[13]. Deterministic models (such as ray-tracing and recording impulse response models) begin by creating an artificial environment. The channel response can be consequently calculated for simulation purposes. But in this case,

the calculation time is considerable high. Geometry-based stochastic channel models (GSCM) consider that the channel response is carried out by respecting the characteristic of wave propagation, both site-specific Tx-Rx environments, and scattering mechanism. All parameters are statistically defined to closely match the measured channel observation. The channel response can be rapidly computed for a single-bounce, double-bounce or multi-bounce scattering mechanism.

Analytical channel models can be further illustrated into correlation-based models, statistical cluster models, and propagation-based models. Correlation-based models contain the Tx and Rx correlations overall channel matrixes. For example, the i.i.d. model is proposed in the case of rich scattering environment with no spatial correlation effect [1], [14], [15]. The kronecker model [16]-[18] assumes that the channel correlation is a product of the correlations at the transmitter and receiver sides. Statistical cluster models determine physical parameters in a random manner without referring to the geometry of a physical medium. For example, Saleh-Valenzuela model [19] uses two exponentially decaying amplitudes varying in time and distance of the clusters, while increasing delay time with the assumptions that the direction of departure (DOD) and the angle of arrival (DOA) are independent and identically distributed. The other models are propagation-based models such as keyhole channel models [20], finite scattered model [21], maximum entropy model [22], virtual channel representation [23] ... etc.

In addition, there are several organizations that proposed different MIMO channel models, systems and algorithms for example COST 207, COST 231, COST 259 [24], COST 273 [25], 3GPP [26] and IEEE 802.16a,e.

1.3 MIMO Channel Capacity

At the end of the 1990s, pioneering works in Bell Labs showed for the first time that the use of multiple antennas at the both sides of the transmission link can result in tremendous channel capacities, provided that the propagation medium is rich scattering [1, 27, 14, 28, 29]. This increase in capacity is obtained without any need to extra bandwidth nor to extra transmission power. Multipath propagation, previously regarded as an impediment to reliable communication, was shown to be exploitable for increasing the data throughput. In this section, we explain briefly how exploiting the spatial dimension can lead to an increase in the system spectral efficiency. Only single-user applications are considered. For more discussions and details, the reader is referred to [15] and the references therein.

1.3.1 Capacity of a fading channel

Let us first recall the definition of the capacity for a fading channel. For a time-varying channel, the capacity C becomes a random variable whose instantaneous value depends on the channel realization [30]. In such a case, the Shannon capacity of the channel may even be zero. Indeed, if we choose a transmission rate for communication, there may be a non-zero probability that the channel realization is incapable of supporting it. The two mostly used definitions for the channel capacity are *ergodic* capacity and *outage* capacity. The ergodic capacity C_{erg}, which is the expected value of C, is suitable for fast varying channels. The outage capacity C_{out} is usually used when considering packet-based transmission systems where the block-fading model properly describes the channel. If the pre-assumed channel capacity is too optimistic, i.e., larger than the instantaneous capacity, a channel outage may occur. The outage capacity, or to say more correctly, the capacity-versus-outage, as seen from its name, is the channel capacity conditioned to an outage probability P_{out}. Obviously, there is a trade-off between the expected data throughput and the outage probability.
In the expressions that we will provide in this section, C will denote the instantaneous channel capacity.

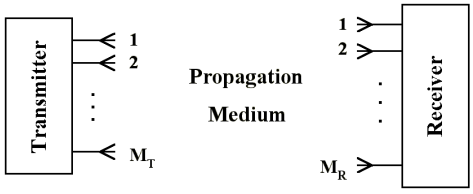

Figure 1.3: Global scheme of a MIMO communication structure

1.3.2 MIMO Capacity

We present the MIMO channel capacity for different cases of channel state information (CSI) at transmitter (Tx) and receiver (Rx).

General assumptions

The global scheme of the transmission link is shown in Fig.1.3. We denote by M_T and M_R the number of antennas at Tx and Rx, respectively. The communication channel includes the effect of transmit/receive antennas and the propagation medium. We neglect the effect of the antenna patterns and assume the *far field* conditions; that is, dominant reflectors are assumed to be sufficiently far from the Tx and the Rx. We consider the simple case of frequency non-selective (flat) fading channel that is true for narrow-band communications. This assumption is mostly valid in indoor applications [31, 32]. In the equivalent baseband representation, each subchannel is characterized by a complex circularly-symmetric random variable that is assumed to be normalized in power. The entire MIMO channel is described by a channel matrix $\boldsymbol{H}$ of dimension $(M_R \times M_T)$. For instance, the entry H_{ij} of $\boldsymbol{H}$, characterizes the subchannel between the i^{th} receive and the j^{th} transmit antenna. Finally, we assume that the total transmit power at each sample time (corresponding to each channel-use) is constrained to P_T.

CSI known to Rx but unknown to Tx

This is the classical case that is usually considered in the literature. The channel is assumed to be known (e.g. perfectly estimated) at the Rx but unknown to the Tx. Since the Tx does

not know the channel, it is logical to distribute the available power uniformly on the transmit antennas. In fact, this is the optimal way for power allotment over the M_T antennas in this case. We denote by ρ_T the total average received signal-to-noise ratio (SNR) at the receiver array $\rho_T = P_T/\sigma_n^2$, where σ_n^2 is the variance of the additive white Gaussian complex noise. The MIMO channel capacity in units of bps/Hz is:

$$C = \log_2 \det \left[\boldsymbol{I}_{M_R} + \frac{\rho_T}{M_T} \boldsymbol{H}\boldsymbol{H}^\dagger \right]. \tag{1.5}$$

Here $\boldsymbol{I}_{M_R}$ is the $(M_R \times M_R)$ Identity matrix. Equation (1.5) can also be written in a different form if we consider the singular value decomposition of $\boldsymbol{H}$:

$$\boldsymbol{H} = \boldsymbol{U}_H \ \boldsymbol{\Lambda}_H \ \boldsymbol{V}_H^\dagger \tag{1.6}$$

where $.^\dagger$ denotes complex conjugate transpose ; $\boldsymbol{U}_H$ and $\boldsymbol{V}_H$ are unitary matrices of dimensions $(M_R \times M_R)$ and $(M_T \times M_T)$, respectively ; and $\boldsymbol{\Lambda}_H$ is an $(M_R \times M_T)$ matrix containing the singular values of $\boldsymbol{H}$. Let us define $M = \min\{M_T, M_R\}$. We denote these singular values by $\lambda_{H,i}$, $i = 1, \cdots, M$. The MIMO capacity can be written in the following form:

$$C = \log_2 \ \det \left[\boldsymbol{I}_{M_R} + \frac{\rho_T}{M_T} \boldsymbol{\Lambda}_H \boldsymbol{\Lambda}_H^\dagger \right] = \sum_{i=1}^{M} \log_2 \left(1 + \frac{\rho_T}{M_T} \lambda_{H,i}^2 \right) \tag{1.7}$$

CSI known to both Tx and Rx

This is the case when the estimated CSI at the Rx is provided for the Tx, which is practically feasible when the channel varies slowly in time. Providing the CSI for the Tx can be done using a (hopefully low bandwidth) feedback channel or via the reverse link when the communication takes place in a duplex mode. We assume that CSI is provided perfectly and without any delay to the Tx. In this case, the Tx can allot the available power on the antennas in an optimal manner in order to achieve the maximum capacity [33]. This capacity is often called *known-CSI* capacity or *water-filling* (WF) capacity. For this purpose, we should weight the transmitted symbols vector $\boldsymbol{x}$ by the matrix $\boldsymbol{V}_H$, and the received signal vector by the matrix $\boldsymbol{U}_H^\dagger$ [15, 34]. This can be regarded as an *optimal beam forming* solution. By

this weighting, we can in fact consider an equivalent channel $\boldsymbol{H}_{eq}$ between $\boldsymbol{x}$ and $\boldsymbol{y}$:

$$\boldsymbol{H}_{eq} = \boldsymbol{U}_H^{\dagger}\ \boldsymbol{H}\ \boldsymbol{V}_H = \boldsymbol{\Lambda}_H\ . \tag{1.8}$$

In other words, the MIMO channel matrix $\boldsymbol{H}$ is decomposed into several parallel independent single-input single-output subchannels. The number of these subchannels is equal to rank($\boldsymbol{H}$), and their gain is given by the singular values of $\boldsymbol{H}$. Let $\boldsymbol{R}_X$ be the autocorrelation matrix of $\boldsymbol{x}$, with eigenvalues $\lambda_{X,i}$, $i = 1, \cdots, M$. The optimal WF solution consists in distributing the available power P_T, optimally over the equivalent parallel subchannels, which results in [15, 35]:

$$\lambda_{X,i} = \left(\psi - \frac{\sigma_n^2}{\lambda_{H,i}^2}\right)^+ \quad , \quad i = 1, \cdots, M \tag{1.9}$$

where, $(s)^+ = s$ if $s > 0$, and 0 otherwise. Also, ψ is a constant which is determined so as to satisfy the constraint on the total transmit power, $\sum_{i=1}^{M} \lambda_{X,i} = P_T$. The WF solution imposes that we allocate more power to best subchannels and lower (or perhaps no) power to worse ones. Now, the WF capacity C_{WF} is given by [15, 35]:

$$C_{\mathrm{WF}} = \sum_{i=1}^{M} \log_2 \left(1 + \frac{\lambda_{X,i}\ \lambda_{H,i}^2}{\sigma_n^2}\right). \tag{1.10}$$

CSI unknown to both Tx and Rx

If channel is not known to the Tx nor to the Rx, we can consider (1.5) as un upper bound on capacity. Let Δ be the coherence interval of the channel in units of channel-uses. As Δ tends to ∞, the channel capacity approaches this upper bound, because with greater Δ, tracking the channel variations becomes more possible for the Rx [36]. For the same reason, there is less difference between the capacity and the upper bound for higher SNR values. This difference becomes more considerable, however, for larger M_T and/or M_R [36]. For a fast varying channel, the capacity is far less than the Rx perfect-knowledge upper bound, because practically there is no possibility to estimate the channel at the Rx. For $M > \Delta$, no increase is achieved in capacity of MIMO channel by increase in M [36]. It is shown in [37]

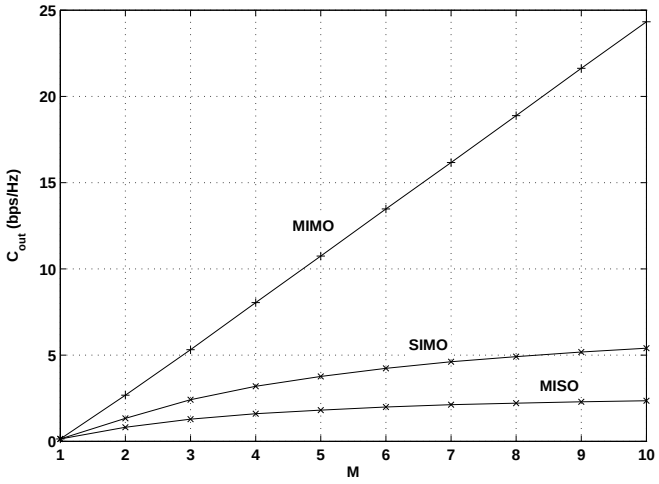

Figure 1.4: Capacity for MIMO, SIMO, MISO structures; uncorrelated Rayleigh flat fading; SNR = 10 dB, $P_{out} = 0.01$.

that at high SNR and for a rich-scattering propagation medium, the MIMO unknown-CSI capacity increases linearly with $M^*(1 - M^*/\Delta)$, where $M^* = \min\{M_T, M_R, \lfloor \frac{\Delta}{2} \rfloor\}$.

1.3.3 Some numerical results

We present some numerical results, excluding the case where CSI is unknown to both the Tx and the Rx. We consider the outage capacity C_{out} for an outage probability of $P_{out} = 0.01$ and will refer to it simply by "capacity." Let us first consider the case where CSI is known only to the Rx. We will call this case *no-WF*. Fig.1.4 contrasts the outage capacity of MIMO, single-input multiple-output (SIMO), and multiple-input single-output (MISO) systems under the conditions of uncorrelated Rayleigh flat fading [38] and $P_{out} = 0.01$. SNR stands for ρ_T. For the MIMO system, we have $M_T = M_R = M$. Uncorrelated fading necessitates enough antenna spacings at the Tx and the Rx that depends, in turn, on the propagation conditions [39, 16]. The MIMO capacity increases linearly with M. It is much more considerable than that of MISO and SIMO systems.

Now consider the case of known-CSI at both the Tx and the Rx. For $M_R \geq M_T$, the improvement in capacity by performing WF, that we call the *WF gain*, is considerable for low SNR and a large number of transmit antennas [33]. But this gain is much more considerable

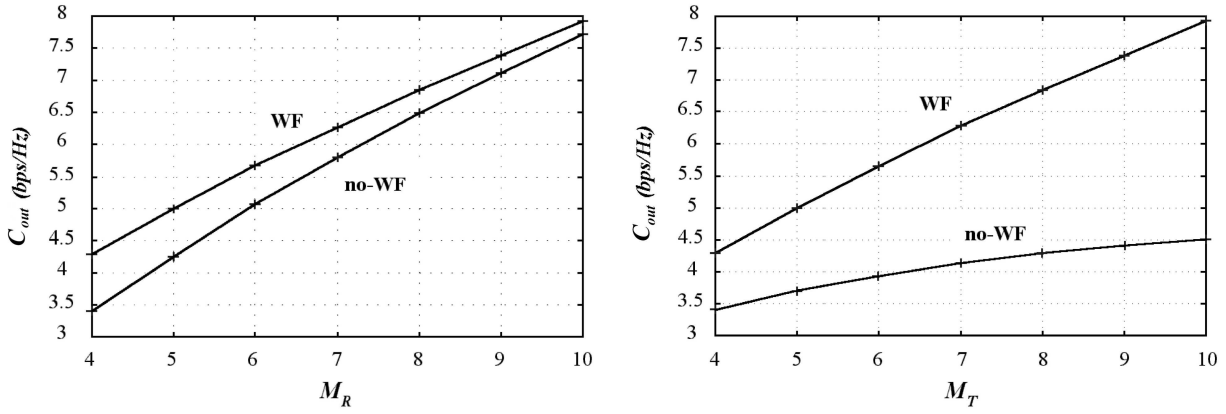

Figure 1.5: WF and no-WF capacities of a MIMO system with $M_R > M_T = 4$ (left) and $M_T > M_R = 4$ (right), Rayleigh flat fading, SNR = 3 dB, $P_{out} = 0.01$.

when $M_T > M_R$. For example, Fig.1.5 shows curves of no-WF and WF capacities for two cases of $M_R > M_T = 4$ and $M_T > M_R = 4$. Notice that the WF-capacity of an (M_T, M_R) system is equal to that of an (M_R, M_T) system. Also, the WF-capacity of a MISO system is equal to that of the equivalent SIMO system.

The gain in capacity by WF is specially interesting for the case of correlated channels. For instance, for the case of Ricean fading [40, 41], curves of capacity versus the Ricean factor (RF) are presented in Fig.1.6 a MIMO system with $M_T = M_R = M$ and two cases of $M = 2$ and $M = 4$. RF represents the percentage of power received from the line-of-sight (LOS) to the total received average power [41]. For relatively high RF that can be regarded as a more correlated channel, the WF gain is quite considerable.

1.4 Iterative Signal Detection

No need to say, signal detection is a crucial part of the transmission system. Among the various detection techniques proposed for the case of MIMO systems, there are iterative (also called *turbo*) detectors. This is what we are going to focus on in this section. In effect, since the invention of turbo-codes by Berrou *et al.* [42] who proposed iterative decoding of parallel concatenated convolutional codes, the *turbo principle* has been applied to several problems in communications such as channel equalization [43], channel estimation [44], synchronization

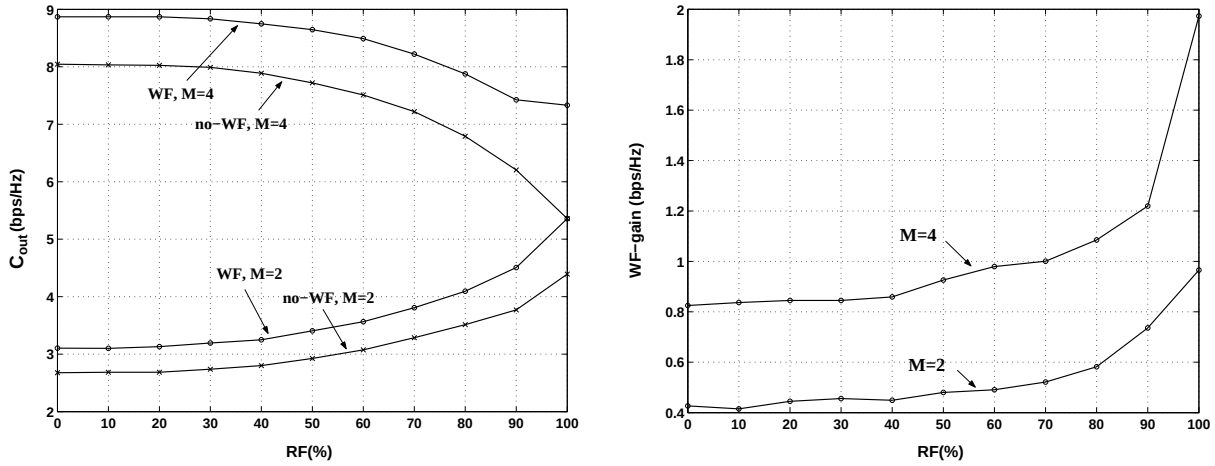

Figure 1.6: WF and no-WF capacities (left) and WF gain in capacity (right) for a MIMO system with $M_T = M_R = M$; Ricean flat fading, SNR = 10 dB, $P_{out} = 0.01$.

[45], multi-user detection [46], and of course to MIMO signal detection [47]. The turbo principle consists of the exchange of *soft* information between two different stages of the Rx, mostly including the soft channel decoder. In MIMO systems too, iterative processing has attracted special attention as it makes a good compromise between complexity and performance. Before presenting the basics of iterative detection, we have to present a brief introduction on space-time coding that is performed at the Tx. We mostly consider frequency non-selective (flat) fading conditions and single-carrier modulation.

1.4.1 Space-time coding and decoding

An important aspect in the implementation of MIMO systems is to appropriately distribute redundancy in space and in time at the Tx, what is called space-time (ST) coding [48]. To this date, there has been considerable work on this subject and a variety of ST schemes has been proposed for MIMO systems. The key criteria in the design of ST codes are the coding gain and the diversity gain. The first one aims at achieving high rate by capitalizing on the MIMO capacity, whereas the latter aims at profiting from the space diversity to reduce fading at the Rx. The two extreme schemes corresponding to these criteria are respectively spatial multiplexing and transmit diversity. For instance, orthogonal space-time block codes (OSTBC) [49, 50] aim at diversity gain and some coding rate; space-time trellis

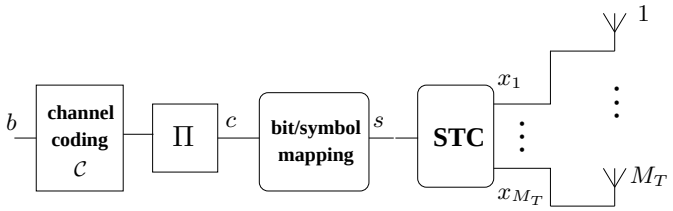

Figure 1.7: Block diagram of the BICM transmission scheme.

codes (STTC) [51] and linear constellation precoding (LCP) [52] aim at both coding and diversity gain; spatial multiplexing or the V-BLAST architecture maximizes the coding rate [28]; and the more general family of linear dispersion (LD) codes [53] that maximize the mutual information between the Tx and the Rx, allow flexible rate-diversity trade-off.
Apart from the problem of code construction, one important criterion in the choice of the appropriate ST scheme could be its decoding complexity. ST orthogonal designs like OSTBCs offer full diversity while they can be decoded using an optimal decoder with linear complexity. However, these schemes suffer from low rate, especially for a large number of transmit antennas. In addition, full-rate OSTBCs exist only for restricted number of transmit antennas and modulations [49]. Non-orthogonal schemes, on the other hand, offer higher coding rates but their optimal decoder becomes prohibitively complex for large number of transmit antennas and large signal constellation sets. This is specially the case for STTC schemes that although offering high rates and good diversity gains, are complex to decode and, moreover, suffer from long decoding delays. For non-orthogonal schemes, instead of performing complex optimal decoding, we may use sub-optimal decoding based on simple linear-algebraic techniques such as sphere decoding [54] or interference-cancelling-based decoding [28, 47]. For either solution, the Rx performance can be improved considerably by performing iterative detection.

ST coding, Tx scheme

In addition to using a special ST scheme, we usually perform channel coding at the Tx. Let us consider bit-interleaved coded modulation (BICM) [55] for which a typical scheme is shown in Fig.1.7. The advantage of the BICM is its flexibility regarding the choice of the code and the bit-symbol mapping, as well as its conformity to iterative detection. In Fig.1.7,

the binary data b are encoded by a channel code $\mathcal{C}$, before being interleaved (the block Π). The output bits c are then mapped to symbols according to a given constellation set. We will mostly consider QAM modulation with B bits per symbol. Power-normalized symbols s are next combined according to a given ST scheme and then transmitted on M_T antennas.

1.4.2 General formulation of LD codes

Before talking about ST decoding, let us present the general formulation of the LD codes from [53] that can be equally used for other ST schemes as well. Let $\boldsymbol{S}$ of dimension $(Q \times 1)$ be the vector of data symbols prior to ST coding:

$$\boldsymbol{S} = [s_1, s_2, \cdots, s_Q]^t, \tag{1.11}$$

where $.^t$ denotes transposition. By ST coding, these symbols are mapped into a $(M_T \times T)$ matrix $\boldsymbol{X}$, where T is the number of channel-uses. We define the ST coding rate as $R_{\text{STC}} = Q/T$. Corresponding to an encoded matrix $\boldsymbol{X}$, we receive the $(M_R \times T)$ matrix $\boldsymbol{Y}$. We separate the $\Re$ and $\Im$ parts of the entries of $\boldsymbol{S}$ and $\boldsymbol{X}$ and stack them row-wise in vectors $\mathcal{S}$ of dimension $(2Q \times 1)$ and $\mathcal{X}$ of dimension $(2M_T T \times 1)$, respectively. For instance,

$$\mathcal{S} = \Big[\Re\{s_1\}\ \Im\{s_1\}, \cdots, \Re\{s_Q\}\ \Im\{s_Q\}\Big]^t. \tag{1.12}$$

We have then, $\mathcal{X} = \mathcal{F}\ \mathcal{S}$, where the $(2M_T T \times 2Q)$ matrix $\mathcal{F}$ depends on the actual ST scheme (see [53] for more details). Let the $(M_R \times M_T)$ matrix $\boldsymbol{H}$ represent our flat channel. Similar to $\mathcal{X}$, we construct the $(2M_R T \times 1)$ vector $\mathcal{Y}$ from $\boldsymbol{Y}$. Vectors $\mathcal{X}$ and $\mathcal{Y}$ are then related through a $(2M_R T \times 2M_T T)$ matrix $\mathcal{H}$:

$$\mathcal{Y} = \mathcal{H}\ \mathcal{X} + \mathcal{N} \tag{1.13}$$

where $\mathcal{N}$ is the vector of real AWGN of zero mean and variance σ_n^2. Matrix $\mathcal{H}$ is composed of $(2T \times 2T)$ segments $\mathcal{H}_{ij}$, $i = 1, \cdots, M_R$, $j = 1, \cdots, M_T$, described below.

$$\mathcal{H}_{ij} = \begin{bmatrix} \boldsymbol{H}_{ij} & 0 & \cdots & 0 \\ 0 & \boldsymbol{H}_{ij} & \cdots & 0 \\ \vdots & & \ddots & \vdots \\ 0 & \cdots & 0 & \boldsymbol{H}_{ij} \end{bmatrix} \tag{1.14}$$

The (2×2) elements $\boldsymbol{H}_{ij}$ are obtained from each entry H_{ij} of the initial matrix $\boldsymbol{H}$:

$$\boldsymbol{H}_{ij} = \begin{bmatrix} \Re\{H_{ij}\} & -\Im\{H_{ij}\} \\ \Im\{H_{ij}\} & \Re\{H_{ij}\} \end{bmatrix}. \tag{1.15}$$

Now, we can describe the "ST encoder and channel" input/output relationship by considering an equivalent channel matrix $\mathcal{H}_{eq}$ of dimension $(2M_RT \times 2Q)$:

$$\mathcal{Y} = \mathcal{H}\ \mathcal{F}\ \mathcal{S} + \mathcal{N} = \mathcal{H}_{eq}\ \mathcal{S} + \mathcal{N}\ . \tag{1.16}$$

1.4.3 Iterative detection for non-orthogonal ST schemes

We assume that $\mathcal{H}_{eq}$ and σ_n^2 are known at the Rx. Having received the vector $\mathcal{Y}$, we should extract from it the transmitted data $\mathcal{S}$. As we perform channel coding together with ST coding, the idea of iterative detection comes into mind. Indeed, by profiting in this way from the channel coding gain, we can obtain a good performance after only few iterations and approach the optimal "ST decoder + channel decoder" performance. This is, of course, the case for non-orthogonal ST schemes. In what follows, we explain the principle of iterative detection and explain in detail the ST decoding part.

The block diagram of such a Rx is shown in Fig.1.8. Soft-input soft-output signal detection and channel decoding are performed. For MIMO signal detection or ST decoding, we can use the optimal maximum *a posteriori* (MAP) algorithm, or a sub-optimal solution based on sphere decoding or interference cancelling, for example. In fact, the optimal MAP detector becomes too complex to implement in practice, especially for large Q or large signal

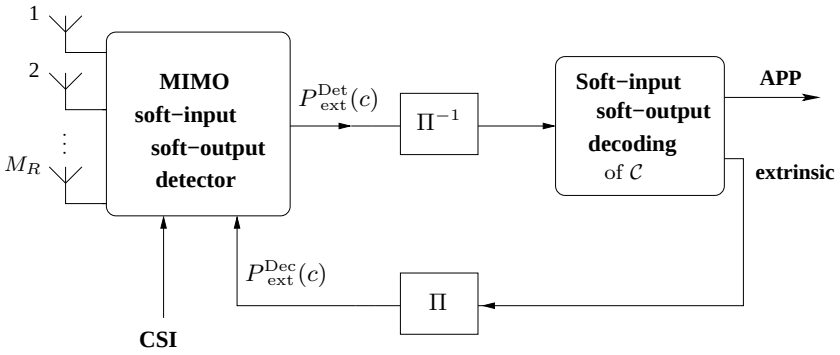

Figure 1.8: Block diagram of the receiver.

constellations.

Soft channel decoding, on the other hand, can be done using the well known forward-backward algorithm [56], the soft-output Viterbi algorithm (SOVA) [57] or a simplification of them [58]. For the final decision making on the transmitted data bits, we use the a posteriori probabilities at the decoder output. Like in any other turbo processing case, *extrinsic* information are exchanged between the two blocks of soft detector and channel decoder. In what follows, we explain the principle of MIMO detection based on MAP, sphere decoding, and soft interference cancelling, while focusing on the third approach.

MAP signal detection

We present here the formulation of the MAP detector based on probabilities. It can also be implemented using logarithmic likelihood ratios (LLR). Remember the expression of $\mathcal{Y}$ from (1.16). The MIMO detector provides at its output extrinsic probabilities on coded bits c. Let $\mathcal{Q}$ be the cardinality of $\mathcal{S}$ of size $q \triangleq |\mathcal{Q}| = 2^{BQ}$. Let also c_i, $i = 1, \cdots, BQ$ be the bits corresponding to a vector of symbols $\mathcal{S} \in \mathcal{Q}$. The extrinsic probability on the bit c_j at the MIMO detector output, $P_{\text{ext}}^{\text{Det}}(c_j)$, is calculated as follows [59]:

$$P_{\text{ext}}^{\text{Det}}(c_j = 1) = K \sum_{\substack{\mathcal{S}\in\mathcal{Q} \\ c_j=1}} \exp\left(-\frac{\|\mathcal{Y} - \mathcal{H}_{eq}\mathcal{S}\|^2}{\sigma_n^2}\right) \prod_{\substack{i=1 \\ i\neq j}}^{BQ} P_{\text{ext}}^{\text{Dec}}(c_i) \tag{1.17}$$

where K is the normalization factor satisfying $P_{\text{ext}}^{\text{Det}}(c_j = 1) + P_{\text{ext}}^{\text{Det}}(c_j = 0) = 1$. The probability $P_{\text{ext}}^{\text{Dec}}(c_i)$ is in fact the *a priori* information on bit c_i, fed back from the channel

decoder. At the first iteration, where no *a priori* information is available on bits c_i, $P_{\text{ext}}^{\text{Dec}}(c_i)$ are set to 1/2. The summation in (1.17) is taken over the product of the conditional channel likelihood (the exponential term) given a vector $\mathcal{S}$, and the *a priori* probability on this symbol, i.e., the term $\prod P_{\text{ext}}^{\text{Dec}}$. In this latter term, we exclude the *a priori* probability corresponding to the bit c_j itself, so as to respect the exchange of *extrinsic* information between the channel decoder and the MIMO detector. Also, this term assumes independent coded bits c_i, which is true for random interleaving of large size.

Sphere decoding

As it was seen, in the calculation of the extrinsic probabilities, the MAP detector considers the exhaustive list of all possibly-transmitted symbol vectors. Hence, the complexity of the MAP detector grows exponentially with the number of transmit antennas M_T and the number of bits per modulation symbol B. By sphere decoding, these probabilities are calculated based on a non-exhaustive list [54]. Corresponding to a vector $\mathcal{Y}$, we only take into account those lattice points that are in a hypersphere of radius R around $\mathcal{Y}$. In this way, the average complexity of the detector under flat fading conditions becomes polynomial (often sub-cubic) [60]. The main detection tasks are then setting the radius R as well as determining which lattice points are within the sphere.

Parallel-Interference-Cancelling-based detection

The block diagram of the detector based on soft-parallel interference cancellation (Soft-PIC) is shown in Fig.1.9. We will refer to the corresponding receiver scheme as turbo-PIC. It is essentially composed of the three blocks of PIC detector, conversion to LLR, and soft-estimation of transmit symbols.

- PIC detector

In order to present general expressions for the detector, let us denote by $\hat{\gamma}_p$, $p = 1, \cdots, 2Q$, the detected data at the PIC detector output, corresponding to the real or imaginary parts of s_q, $q = 1, \cdots, Q$. At the first iteration, $\hat{\gamma}_p$ are obtained via MMSE (minimum mean-square

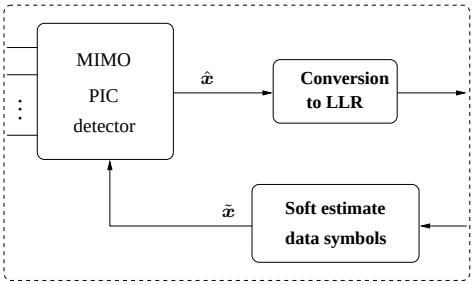

Figure 1.9: Block diagram of the Soft-PIC detector

error) filtering [47, 61, 62].

$$\hat{\gamma}_p = \mathcal{W}_p^{\dagger}\ \mathcal{Y} = h_p^{\dagger}\big(\mathcal{H}_{eq}\mathcal{H}_{eq}^{\dagger} + \sigma_n^2\boldsymbol{I}\big)^{-1}\ \mathcal{Y} \tag{1.18}$$

where $\mathcal{W}_p$ denotes the filter, h_p is the p^{th} column of $\mathcal{H}_{eq}$, and $(.)^{\dagger}$ stands for transpose complex conjugate. Note that the entries of $\mathcal{H}_{eq}$ are real values, and hence, $(.)^{\dagger}$ is equivalent to transposition. From the second iteration, we can calculate soft estimates $\tilde{\mathcal{S}}$ of the transmitted data using the soft decoder outputs. Using these estimates, we perform interference cancelling followed by a simple inverse (zero-forcing) or MMSE filtering:

$$\hat{\mathcal{Y}}_p = \mathcal{Y} - \mathcal{H}_p\ \tilde{\mathcal{S}}_p \quad , \quad \hat{\gamma}_p = \mathcal{W}_p^{\dagger}\ \hat{\mathcal{Y}}_p \tag{1.19}$$

$$\text{ZF: } \mathcal{W}_p = \frac{1}{h_p^{\dagger}\ h_p}\ h_p \qquad , \qquad \text{MMSE: } \mathcal{W}_p = \frac{1}{(h_p^{\dagger}\ h_p + \sigma_n^2)}\ h_p \tag{1.20}$$

where $\tilde{\mathcal{S}}_p$ of dimension $((2Q-1)\times 1)$ is $\tilde{\mathcal{S}}$ with its p^{th} entry removed, and $\mathcal{H}_p$ of dimension $(2M_RT \times (2Q-1))$ is the matrix $\mathcal{H}$ with its p^{th} column removed. Notice that, compared to the exact MMSE filtering proposed in [47], (1.20) are simplified solutions that assume almost perfect estimation of data symbols and permit a considerable reduction of the computational complexity. Thanks to iterative processing, the performance loss due to this simplification would be negligible. In the results that we present later, we will consider the simplified ZF solution.

• Conversion to LLR

For QAM modulation with B (an even number) bits per symbol, we can attribute $m = B/2$ bits to the real and imaginary parts of each symbol. Let for instance, the bit c_i corresponds

to the real (imaginary) part of the symbol s_q. Let also $a_{1,j}$ and $a_{0,j}$, $j = 1, \cdots, \frac{B}{2}$ denote the real (imaginary) part of the signal constellation points, corresponding to $c_i = 1$ and $c_i = 0$, respectively. Remember that the signal constellation points have normalized average power. The LLR corresponding to c_i is calculated as follows [61]:

$$\mathrm{LLR}_i = \log_{10} \frac{\sum_{j=1}^{2^{m-1}} \exp\left(-\frac{1}{2\sigma_p^2}(\hat{\gamma}_p - a_{1,j})^2\right)}{\sum_{j=1}^{2^{m-1}} \exp\left(-\frac{1}{2\sigma_p^2}(\hat{\gamma}_p - a_{0,j})^2\right)}, \; i = 1, \cdots, m \tag{1.21}$$

where σ_p^2 is the variance of noise plus the residual interference (RI) that intervenes in the detection of $\hat{\gamma}_p$, and assumed to be Gaussian. Note that, as the detection is performed on blocks of Q complex symbols, or in other words on blocks of $2Q$ *real symbols* in our model, the RI comes in fact from $(2Q-1)$ other real symbols in the corresponding channel-use [63]. In LLR calculation, we need the variances σ_p^2. These variances can be calculated analytically as shown in [64], or estimated at each iteration and for each one of $2Q$ real symbols, as done in [63]. To simplify the detector further, we may neglect the RI and take only into account the noise variance. For not too large signal constellation sizes, this simplification causes a negligible performance loss [65, 66].

• Soft estimation of transmit symbols

Each element $\tilde{\gamma}_p$ of the vector $\tilde{\mathcal{S}}$ is obtained by taking a summation over the all possible values of the real part (or imaginary part) of the signal constellation, multiplied by the corresponding probability calculated using the soft decoder output [61, 62]. It is preferable to use the a posteriori information from the decoder output rather than extrinsic information in the calculation of $\tilde{\gamma}_p$. This has the advantage of permitting a better and faster convergence of the Rx.

Case study

As we focus here on the turbo-PIC detector as the sub-optimal solution, we just compare the performance of this detector with that of turbo-MAP. We consider the simplified implementation of Soft-PIC based on ZF filtering given in (1.20). For this comparison, we consider

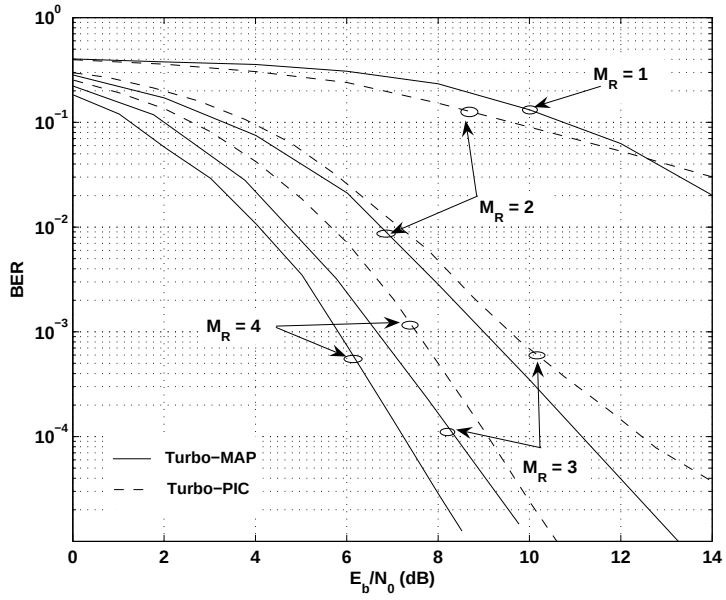

Figure 1.10: Comparison of turbo-PIC and turbo-MAP detectors, $M_T = 4$, $(5,7)_8$ channel code, QPSK modulation, 64 channel-uses per frame.

the simple spatial multiplexing (V-BLAST) ST scheme and the case of a four-transmit antennas, $M_T = 4$ while we take M_R between 1 and 4. The Tx and the Rx schemes correspond to Figures 1.7 and 1.8, respectively. We consider Gray bit/symbol mapping and random interleaving, as well as the Rayleigh flat quasi-static channel model. The non-recursive and non-systematic convolutional (NRNSC) channel code $(5,7)_8$ (in octal representation) is considered with rate $R_c = 1/2$. SNR is considered in the form of E_b/N_0, where E_b is the average received energy per information bit and N_0 is the unilateral noise power spectral density; E_b/N_0 includes the Rx array gain, M_R.

Curves of bit-error-rate (BER) versus E_b/N_0 are given in Fig.1.10. It fact, the performance of turbo-PIC and turbo-MAP are relatively close to each other for $M_R \geq M_T$. Turbo-PIC can still be used for certain values of $M_R < M_T$, mostly for $M_R > M_T/2$ [62]. So, for these M_R values where turbo-PIC converges properly, it would be preferred to turbo-MAP due to its considerably lower complexity. Better performances are obtained for turbo-PIC if the variance of the RI is taken into account in LLR calculation [62].

1.4.4 Orthogonal versus non-orthogonal ST schemes

In practice, to attain a desired spectral efficiency, we should adopt the most appropriate scheme by fixing the degrees of freedom of the system, that is, the signal constellation, the channel coding rate, and the ST coding scheme. The answer to the question "what is the most suitable combination" is not obvious for moderate to high spectral efficiencies. In effect, if a low spectral efficiency is required, an OSTBC scheme together with a powerful turbo-code would be a suitable solution, as the reduction in the overall coding rate is best invested in turbo channel codes [67]. To attain high spectral efficiencies with OSTBC schemes, however, we have to use large signal constellations and to increase the channel coding rate by puncturing the encoder output bits. Use of larger signal constellations complicates the tasks of synchronization and detection at the Rx and also results in a higher SNR required to attain a desired BER. On the other hand, puncturing results in a reduced channel code robustness against noise. Higher ST coding rates are offered by non-orthogonal schemes, hence, relaxing the conditions on signal constellation and channel coding. Here, a simple (sub-optimal) iterative detector can be used for ST decoding, as explained in the previous subsection, and we may approach the optimal detection performance after few iterations. Nevertheless, the detector remains more complex, as compared to the OSTBC case. However, this increased Rx complexity is quite justified; using such an appropriate non-orthogonal ST scheme and iterative detection, we obtain a considerable gain in performance with respect to OSTBC choice [63, 65, 66]. Results in [65, 66] have also confirmed that the gain obtained by using non-orthogonal with respect to orthogonal schemes is still considerable and even more important when channel estimation errors are taken into account.

• Case study

We consider again the case of a (2×2) MIMO system, Gray bit/symbol mapping and random interleaving, as well as the Rayleigh flat block-fading channel model with $N_c = 32$ independent fades per frame. The number of channel-uses corresponding to a frame is 768. The NRNSC channel code $(133, 171)_8$ is considered with rate $R_c = 1/2$. ST schemes we consider are resumed in Table I, where η is the spectral efficiency in units of bps/Hz. As the OSTBC scheme, we consider the Alamouti code [50]. Using the formulation of LD codes that we

Table 1.1: Different ST schemes for a (2×2) MIMO system with $\eta = 2$ bps/Hz

ST scheme	R_{STC}	Modulation	R_c
Alamouti	1	16-QAM	1/2
V-BLAST	2	QPSK	1/2
GLD	2	QPSK	1/2

presented in Subsection 1.4.2, we have $Q = T = 2$, $R_{\text{STC}} = 1$, and:

$$\boldsymbol{X} = \begin{bmatrix} s_1 & s_2 \\ -s_2^* & s_1^* \end{bmatrix}. \tag{1.22}$$

For the OSTBC case, the decoding is performed once using (1.18). We also consider two non-orthogonal schemes. The first one is the simple V-BLAST scheme described by $\boldsymbol{X} = [\, s_1 \;\; s_2 \,]^t$ for which $Q = 2,\ T = 1$ and $R_{\text{STC}} = 2$. The second one is the optimized scheme proposed in [68] and called *Golden code* that we denote by GLD. For this code that offers full-rate and full-diversity with the property of non-vanishing determinant, we have $Q = 4$, $T = 2$, and $R_{\text{STC}} = 2$:

$$\boldsymbol{X} = \frac{1}{\sqrt{5}} \begin{bmatrix} \alpha\ (s_1 + \theta\ s_2) & \alpha\ (s_3 + \theta\ s_4) \\ \gamma\ \overline{\alpha}\ (s_3 + \overline{\theta}\ s_4) & \overline{\alpha}\ (s_1 + \overline{\theta}\ s_2) \end{bmatrix}, \tag{1.23}$$

where $\theta = \frac{1+\sqrt{5}}{2},\ \alpha = 1 + j(1-\theta),\ \overline{\theta} = 1 - \theta,\ \overline{\alpha} = 1 + j(1-\overline{\theta}),\ \gamma = j = \sqrt{-1}$. The factor $1/\sqrt{5}$ ensures normalized transmit power per channel-use. For $\eta = 2$ bps/Hz, performance curves are shown in Fig.1.11, where again perfect channel knowledge is assumed at the Rx. For V-BLAST and GLD schemes, BER curves are shown for the second and the fourth iteration where almost full Rx convergence is attained. We see that, by using V-BLAST scheme, we gain about 3.3 dB and 3.75 dB in SNR at BER$= 10^{-4}$ after two and four iterations, respectively, compared to Alamouti coding. The corresponding gains by using GLD code are about 3.5 dB and 4.3 dB, respectively. We note that even when for the reasons of complexity and/or latency, only two iterations are to be performed, the gain in SNR compared to Alamouti scheme is still considerable.

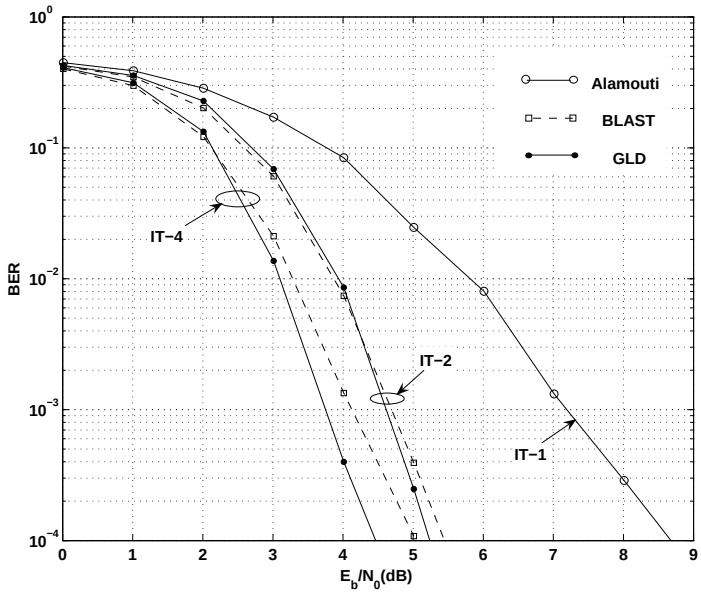

Figure 1.11: (2×2) MIMO system, Turbo-PIC detection, $(133, 171)_8$ channel code, $\eta = 2$ bps/Hz

1.5 Advanced Polarization Diversity Techniques for MIMO Systems

For next-generation wireless communication systems, multiple antennas at both transmitter and receiver could be used to achieve a higher capacity and reliability of wireless communication channels under rich scattering environments. With multiple antenna communication systems, the performance could moreover be improved on a limited bandwidth and transmission power.

Due to the potential of MIMO systems, the initial research demonstrates that the channel capacity based on uncorrelated channel model can be proportionally increased with respect to the number of antennas. However, in practice, the performance of MIMO communication channel are affected by the spatial correlation, which is dependent on antenna array configurations (such as radiation pattern, antenna spacing and array geometry), and propagation channel characteristics, which are dependent on the environment, (such as number of channel paths, distribution and properties of scatterers, angle spread and cross-polarization discrimination). Thus, the antenna arrays at transmitter and receiver should be properly designed to reduce the spatial correlation effects and to improve the communication performance.

However, it is possible to reduce these effects by increasing antenna array spacing but this solution is not always suitable in some wireless applications where the array size is limited. Therefore, in order to eliminate the spatial correlation effects and remain with high transmission performance, there are essentially two diversity techniques such as angular [69] and polarization diversity techniques [70]. For pattern diversity technique, the radiation of antennas should be generated in a manner to isolate the radiation pattern. For polarization diversity techniques [71], the antennas are designed to radiate with orthogonal radiation polarizations to create uncorrelated channels across different array elements. The polarization diversity techniques could be applied in point-to-point communication systems such as Inter Mobile Base Station Communications, Mobile Satellite Communications, High Resolution Localization Systems, Military Communications, etc.

Finally, there are also other diversity techniques; such as multimode diversity [72] that exploits the difference of high order modes to obtain low correlated channels across the modes and a combination of pattern and polarization diversity techniques [73], [74] that take together the advantages of orthogonal radiation patterns and polarizations.

1.5.1 Antennas

In pratice, not only the propagation environment for the multiple antenna systems has an important role in determining the transmission performance, but also the proper implementation of the antennas plays another dominant role. For example uniform linear arrays, uniform circular arrays and cube antenna arrays give different performances in terms of channel capacity. Moreover, different array configurations produce different correlation effects. In this part, we will analyze five types of antennas [75] such as x-, y- and z- oriented dipole antennas, azimuth, and elevation isotropic antennas are applied to a uniform linear array.

Table 1.2: Patterns of different electric dipoles

	E_x	E_y	E_z	E_ϕ	E_θ
$E_\theta(\theta,\phi)$	$-cos\theta cos\phi$	$-cos\theta sin\phi$	$-sin\theta$	0	1
$E_\phi(\theta,\phi)$	$sin\phi$	$-cos\phi$	0	1	0

The radiating patterns of the antennas are considered in the far field case, and also simplified by neglecting path loss and distance phase. Hence, these radiating patterns are simply dependent on the azimuth and elevation angle direction as shown in table 1.2. A general expression of radiation patterns is given by [75]

$$E = E_\theta(\theta,\phi)\vec{\theta} + E_\phi(\theta,\phi)\vec{\phi} \tag{1.24}$$

where $E_\theta(\theta,\phi)$ and $E_\phi(\theta,\phi)$ are the amplitudes of polarization vector at $\vec{\theta}-$ and $\vec{\phi}-$direction, and x, y and z are the antenna orientations. As different types of antenna are employed in this paper, it is necessary to normalize the radiation pattern when comparing all channel performances. Thus all radiation patterns of an antennas are normalized by that of isotropic

antenna, and they can be written as

$$G = \sqrt{\frac{\int\int\limits_{\Delta\phi,\Delta\theta} \sin\theta d\theta d\phi}{\int\int\limits_{\Delta\phi,\Delta\theta} \left[\left|E_\theta\left(\theta,\phi\right)\right|^2 + \left|E_\phi\left(\theta,\phi\right)\right|^2\right] \sin\theta d\theta d\phi}} \left(E_\theta\left(\theta,\phi\right)\vec{\theta} + E_\phi\left(\theta,\phi\right)\vec{\phi}\right) \tag{1.25}$$

where G is the antenna gain that is used for the computation of the channel matrix.

1.5.2 Cross polarization discrimination

In wireless communications, due to the interactions of environment such as diffractions, reflection and refraction, the transmitted signals are generally not only attenuated, but also depolarized. Depolarization is the change of the original state of the polarization of the electromagnetic wave propagated from the transmitter.

Cross-polarization discrimination (XPD) is defined as the power ratio of the co-polarization and the cross-polarization components of the mean incident wave. The higher the XPD, the less energy is coupled in the cross-polarized channel. Therefore, there are two transmission cases namely azimuth transmission (χ_θ) and elevation transmission (χ_ϕ) as follows

$$\chi_\theta = \frac{E\left\{\left|E_{\theta\theta}\right|^2\right\}}{E\left\{\left|E_{\theta\phi}\right|^2\right\}}, \quad \chi_\phi = \frac{E\left\{\left|E_{\phi\phi}\right|^2\right\}}{E\left\{\left|E_{\phi\theta}\right|^2\right\}} \tag{1.26}$$

where $E_{\theta\phi}$ denotes the θ-polarized electric field which is propagated from a transmitter and received in the ϕ polarization. It has the same explanation for $E_{\theta\theta}$, $E_{\phi\phi}$ and $E_{\phi\theta}$. In the literature, some measurement campaigns have been carried out and they concluded that the XPD depended on the physical obstacles, the distance between transmitter and receiver and the delay of multipath components of each environment [76]. Therefore, for simplicity, XPD can be approximated by a Gaussian statistical distribution with average μ and variance σ^2 [77] ,[78]. For urban environment, the mean value of XPD can vary from 0 to 16 dB and the standard deviation can change from 3 to 9 dB.

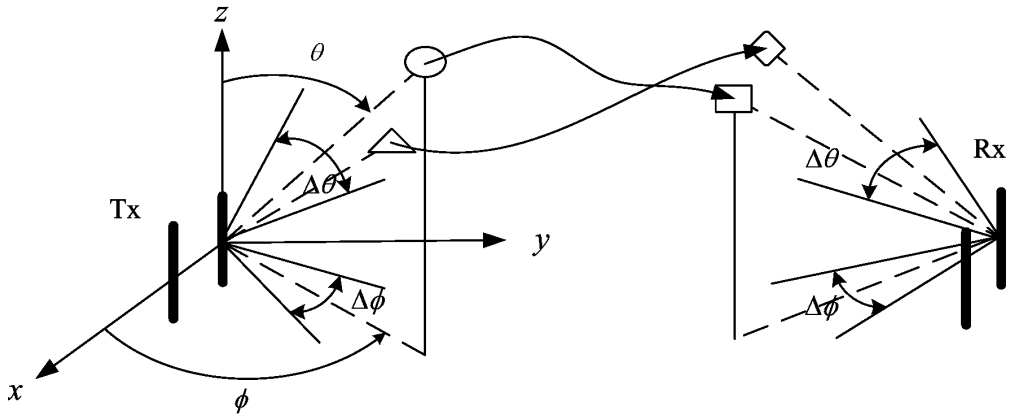

Figure 1.12: Geometries of MIMO channel

1.5.3 Geometry-based stochastic channel models

We now focus on a useful model for simulation purposes, geometry-based stochastic modelling or geometric scattering modelling [10],[79],[80], which can be easily exploited to examine the performance of different antenna patterns and polarizations. This model is based on the assumption that scatterers around the transmitter and receiver influence the direction of departure (DOD) and the direction of arrival (DOA) respectively within transmit and receive scattering areas. Scatterers are randomly located according to a certain probability distribution. In particular, the scatterers are used to represent the depolarization and attenuation mechanism of incident waves travelling from the transmitters.

In Fig.1.12, a scattering geometry is shown. A uniform linear array of z-oriented dipole antennas at both transmitter and receiver is employed. The height of transmitter and receiver has the same level. Moreover, transmit and receive scatterers are uniformly distributed within an angular region defined by $|\phi + \pi/2| \leq \Delta\phi/2$ in elevation area and $|\theta + \pi/2| \leq \Delta\theta/2$ in azimuth area. In order to determine one propagation path, from one transmit scatterer to one receive scatterer, we consider that there is a double depolarization mechanism replaced by one scattering matrix. One of the propagation path channels occurs when one of transmit and one of receive scatterers are randomly linked. To reduce the computational cost, a scatterer is used to generate only one propagation channel. Then the actual channel impulse response is established by a sum of propagation channels. We also assume that the channel

coherence bandwidth is larger than the transmitted bandwidth of the signal. This channel is usually called frequency non-selective or flat fading channel.

In case of far field transmission without the line-of-sight channel, the flat fading transmission channel between the antenna p at the transmitter and the antenna m at the receiver can be expressed as

$$\begin{array}{l} h_{mp}(t,f) = \frac{1}{\sqrt{N_S}} \sum_{i=1}^{N_S} a_m^{(i)} a_p^{(i)} \exp\left\{-j\vec{k}^{(i)} \cdot \vec{v}_{Rx} t - j\vec{k}'^{(i)} \cdot \vec{v}_{Tx} t + \varphi_{mp}\right\} \\ \left[G_\theta^m(\theta_i,\phi_i) \quad G_\phi^m(\theta_i,\phi_i)\right] \mathbf{S}_{mp}^{(i)} \begin{bmatrix} G_\theta^p(\theta_i,\phi_i) \\ G_\phi^p(\theta_i,\phi_i) \end{bmatrix} \end{array} \tag{1.27}$$

where

- t is time;
- f is frequency;
- N_S is the number of scatterers at the receiver and the transmitter;
- $\vec{v}_{Rx}$ and $\vec{v}_{Rx}$ are the velocity vector of the transmitter and the receiver;
- $\vec{k}'^{(i)}$ and $\vec{k}^{(i)}$ are the vectors of wave number in the direction of the ith transmit scatterer and the ith receive scatterer where $\left|\vec{k}^{(i)}\right| = \left|\vec{k}'^{(i)}\right| = 2\pi/\lambda$;
- $G_\theta^p(\theta_i,\phi_i)$ and $G_\phi^p(\theta_i,\phi_i)$ are the gain in the $\vec{\theta}$ and $\vec{\phi}$ directions of the pth transmit antenna in the direction of the ith transmit scatterer;
- $G_\theta^m(\theta_i,\phi_i)$ and $G_\phi^m(\theta_i,\phi_i)$ are the gain in the $\vec{\theta}$ and $\vec{\phi}$ directions of the mth receive antenna in the direction of the ith receive scatterer;
- $a_m^{(i)}$ is the mth element of the local vector of the receive antenna, so that the local receive vector can be expressed as $\mathbf{a}_{\mathrm{Rx}}^{(i)} = \left[1 \quad \exp\left\{-j\vec{k}^{(i)} \cdot \vec{r}_1\right\} \cdots \exp\left\{-j\vec{k}^{(i)} \cdot \vec{r}_{M_R-1}\right\}\right]$;
- $a_p^{(i)}$ is the pth element of the local vector of the transmit antenna, so that the local transmit vector can be expressed as $\mathbf{a}_{\mathrm{Tx}}^{(i)} = \left[1 \quad \exp\left\{-j\vec{k}'^{(i)} \cdot \vec{r}'_1\right\} \cdots \exp\left\{-j\vec{k}'^{(i)} \cdot \vec{r}'_{M_T-1}\right\}\right]$;
- $\mathbf{S}_{mp}^{(i)}$ are a 2×2 scattering matrix for the ith transmit scatterer and the ith receive scatterer for i $= 1 \ldots N_S$ wave components. Scattering matrix contains the polarization mechanism as defined by

$$\mathbf{S}_{mp}^{(i)} = \begin{bmatrix} \sqrt{\frac{\chi_\theta}{1+\chi_\theta}} \exp\left\{j\beta_{mp}^{(\theta\theta)}\right\} & \sqrt{\frac{1}{1+\chi_\phi}} \exp\left\{j\beta_{mp}^{(\phi\theta)}\right\} \\ \sqrt{\frac{1}{1+\chi_\theta}} \exp\left\{j\beta_{mp}^{(\theta\phi)}\right\} & \sqrt{\frac{\chi_\phi}{1+\chi_\phi}} \exp\left\{j\beta_{mp}^{(\phi\phi)}\right\} \end{bmatrix} \tag{1.28}$$

where $\beta_{mp}^{(\phi\theta)}$ denotes phase offset of ith incident wave which changes from $\vec{\phi}$ directions to $\vec{\theta}$ directions superposing on m-p channel and χ_θ and χ_ϕ denote the ratio of the co-polarized average received power to the cross-polarized average received power. In [77], after sufficiently reflecting the propagation signal between transmitters and receivers, the polarization state of the signal will be independent of the transmitted signals.

1.5.4 Spatial correlation and angle spread effects

The consecutive MIMO systems based on spatial diversity technique are directly influenced by spatial correlation effect (or antenna correlation effect) [16]. This effect is drastically dependent on array configurations and environment characteristics. Therefore, the antenna arrays at both transmitter and receiver should be properly designed or adapted to decrease spatial correlation effects.

As illustrated in Fig.1.13, the spatial correlation of 2×2 uniform linear antenna array depends on the antenna spacing and the angle spread (AS). The general expression of spatial correlation [81] between two antenna elements can be written as

$$\rho_{ij} = \frac{\int\int\limits_{\Delta\theta,\Delta\phi} a_i \cdot a_j^* \sin(\theta)\, p(\theta,\phi)\, d\theta d\phi}{\sqrt{\int\int\limits_{\Delta\theta,\Delta\phi} |a_i|^2 \sin(\theta)\, p(\theta,\phi)\, d\theta d\phi \cdot \int\int\limits_{\Delta\theta,\Delta\phi} |a_j|^2 \sin(\theta)\, p(\theta,\phi)\, d\theta d\phi}} \tag{1.29}$$

where a_i is local value of the ith transmit or receive antenna and a_j is local value of the jth transmit or receive antenna in local vector. The scalar $p(\theta,\phi)$ is the joint probability density function (pdf) of the angles of arrival for the receiving spatial correlations or of the angles of departure for the transmitting spatial correlations.

When the narrow angle spread of incident fields occurs in the transmitting or receiving side, the separation between antennas should be expanded in order to reduce the spatial correlation problem as shown in Fig.1.13. This shows the spatial correlation of 2×2 MIMO z-oriented antennas in the case of a uniform distribution of the angles of arrival within a

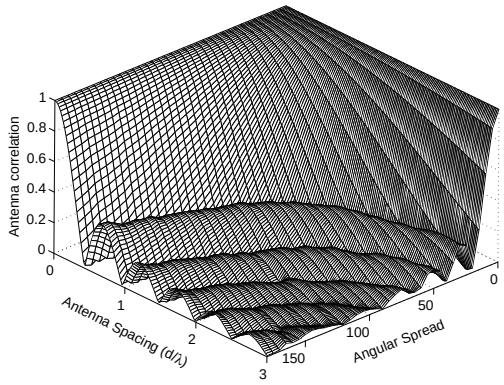

Figure 1.13: Spatial correlation of uniform linear antenna array for single-polarized configuration

region. It demonstrates that the received signals become uncorrelated when the antenna spacing is sufficiently increased and the angle spread is quite wide.

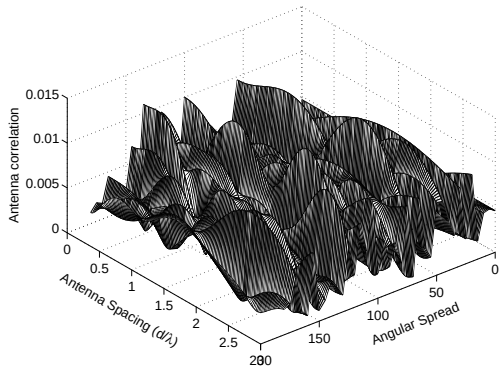

Figure 1.14: Spatial correlation of uniform linear antenna array for dual-polarized configuration

However, wide antenna spacing may preclude implementation is some applications where size is a limitation. The use of polarized antennas is promising low spatial correlation. The spatial correlation is demonstrated in Fig.1.14 while 2×2 polarized MIMO configuration employs a pair of y- and z-oriented dipole antennas at both Tx and Rx. The spatial correlation of dual-polarized MIMO is much lower than that of single-polarized MIMO in all simulation scenarios.

Although there are only two diversity branches, it does allow the antenna elements to be colocated without the correlation effect. However, there is considerable interest in many di-

versity branches by applying a combination of the pattern and polarization diversity [82],[74].

1.5.5 Capacity of polarized channels

Antenna polarization diversity is very useful in MIMO systems for enhancing channel capacity. Indeed, employing polarization diversity can reduce the antenna array size and also the spatial correlation, then we can obtain a better capacity. That is why the multi-polarized antennas become more and more interesting in MIMO transmission systems. In this section, MIMO systems are investigated to show the potential of using multi-polarized antennas for differently oriented dipole antennas.

We consider that channel state information (CSI) is perfectly known to the receiver but unknown to the transmitter. This is in theory what happens to signals propagating through an urban and an indoor environment. In the case of a random channel model, the channel matrix (1.27) is stochastic and then the capacity given by (1.5) is also random. In this situation, the ergodic capacity can be obtained by taking the expectation of capacity over all possible channel realizations.

Fig.1.15 demonstrates the 2×2 MIMO channel capacity of isotropic antennas with single-polarization in (a) and with dual-polarization in (b). In this case, the single polarization configuration exploits only azimuth isotropic antenna and the dual polarization configuration applies azimuth and elevation isotropic antennas. The channel capacity is examined in function of angular spread (AS) with 20 scatterers distributed around the transmitter and receiver. As mentioned in the previous section, the XPD is defined for the urban case by χ_θ and $\chi_\phi \sim \mathcal{N}(0, 9)$. As shown in Fig.1.15a, the MIMO channel capacity increases as the angle spread increases at transmitter and receiver for the same polarization antennas. In contrast, dual polarization improves the channel capacity due to the lower antenna correlation as shown in Fig.1.15b. However, when the spatial correlation of the single-polarized antennas is lower, the channel capacity is proportional until 6.7 dB for AS$>$ 80°. It should be noted that the MIMO channel capacity is significantly dependent on the antenna correlation.

Fig.1.16 shows the difference between the triple-polarized and the single-polarized channel

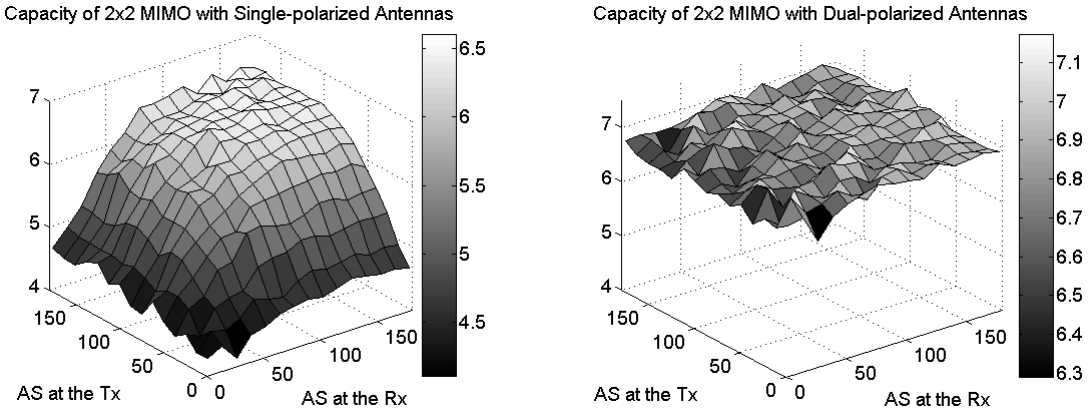

(a) (b)

Figure 1.15: 2×2 MIMO channel capacity of isotropic antennas: (a) single-polarization configuration and (b) dual-polarization configuration

capacity ($\Delta C = C_{\text{triple-polar}} - C_{\text{single-polar}}$) of 3×3 MIMO system versus the average XPD and AS. The propagation environment has the same conditions as the previous section. For triple-polarization configuration, x-, y- and z-oriented dipole antennas are employed. This can represent a combination of angular and polarization techniques. We found that for the triple-polarization case, the average power of subchannel can be unfortunately loosed when the angular spread is not large enough until covering all antennas. As seen in Fig.1.16, the single-polarized channel capacity can be superior to the triple-polarized channel capacity because single polarization has a low spatial correlation and triple polarization loses the subchannel power due to insufficient angular spread. However, generally speaking for most scenarios, triple polarizations can maintain a higher capacity with respect to the single polarization case.

1.5.6 Impact of depolarization effect on MIMO configurations

In this section, we investigate the impact of the depolarization effect on 4×4 MIMO systems with single- and dual-polarization configurations. While pattern and polarization diversity techniques are employed, the special correlation effect can be reduced or eliminated when there is no-pattern interference. Nevertheless, the cross-polarization discrimination (XPD) becomes the most important parameter because XPD represents the ratio of the co-polarized

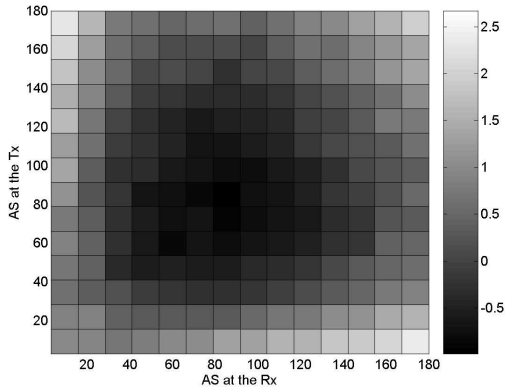

Figure 1.16: Difference between the triple-polarized and the single-polarized channel capacity of 3×3 MIMO system employing the dipole antennas

average received power to the cross-polarized average received power. Then, for a high XPD value, less energy is coupled between the cross-polarized wireless channels. At lower XPD and higher K-factor values [83], multi-polarized antenna arrays can give high capacity. However, at higher XPD and lower spatial correlation, a single-polarized antenna array can provide even better results.

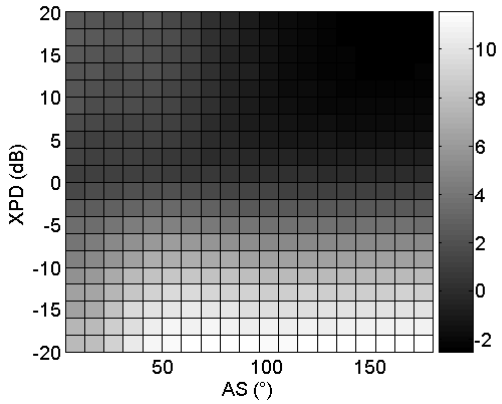

Figure 1.17: Difference between the dual-polarized and the single-polarized channel capacity of 4×4 MIMO systems in the functions of XPD and AS

Fig.1.17 explains the difference between the dual-polarized and single-polarized channel capacity ($\Delta C = C_{\text{dual-polar}} - C_{\text{single-polar}}$) of 4×4 MIMO systems versus XPD and AS. Same angle spreads at transmitter and receiver is considered in the simulation. For high XPD and sufficiently large angle spread, we can note that the MIMO channel capacity of the single-polarized antenna is superior to that of the dual-polarized antenna because of the

subchannel power loss. The Frobenius norm of MIMO channel is used to investigate the total channel power. It confirms that with a high XPD and low spatial correlation the average transmission power of single-polarized isotropic antenna arrays is $\|\boldsymbol{H}\|_F \approx MN$ but that of dual-polarized isotropic antenna arrays is always $\|\boldsymbol{H}\|_F \approx M^\theta N^\theta + M^\phi N^\phi$ for high XPDs and $\|\boldsymbol{H}\|_F \approx M^\theta N^\phi + M^\phi N^\theta$ for low XPDs.

Fig.1.18 shows the XPD impact on 4×4 MIMO systems with single- and dual-polarization configurations. We employ four azimuth isotropic antennas for the single-polarization configuration and two elevation and two azimuth isotropic antennas for the dual-polarization configurations, which are applied to a uniform linear antenna array with a $\lambda/2$ antenna separation. It shows that the channel power of single-polarization configuration augments significantly with respect to XPD until $\|\boldsymbol{H}\|_F$=4×4=16, while for that of dual-polarization configuration keeps around $\|\boldsymbol{H}\|_F$=2×2+2×2=8.

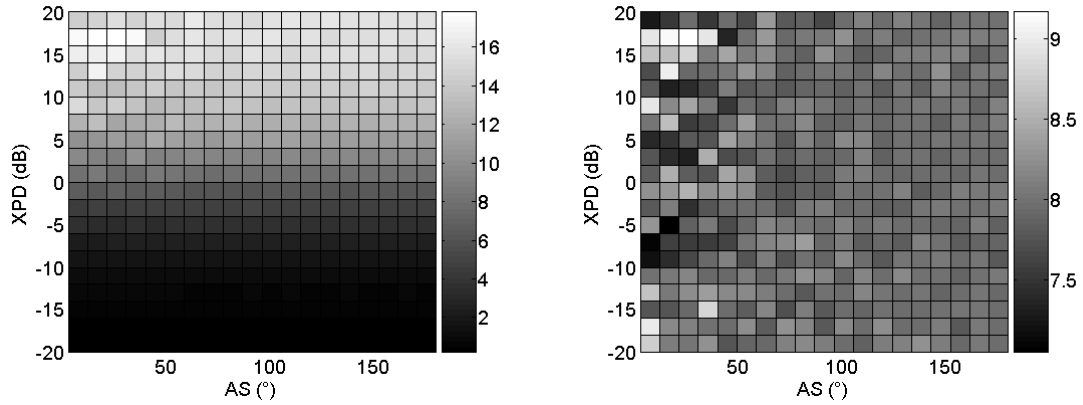

(a) (b)

Figure 1.18: Frobenius norm of 4×4 MIMO systems in terms of XPD and AS with: (a) a single-polarization configuration and (b) a dual-polarization configuration

1.5.7 Adaptive MIMO polarized-antenna selection technique(AMPAS)

In the previous sections, we defined the scattering mechanisms which are used to represent not only the attenuation of traveling waves but also the polarization of the electromagnetic wave. The achieved performance in capacity is calculated under the assumption that the average received power is normalized and the channel attenuation is neglected. Subsequently,

the variation of polarization is characterized only by the XPD effects.

As shown in Fig.1.17, this phenomenon affects directly the performance of non-polarized MIMO systems. In single-polarization communications case, low XPD causes higher losses in channel power, in other words there is some sort of mismatch in polarization. That is why we will apply adaptive techniques to reduce this mismatch in the polarization of MIMO systems. This technique is called adaptive MIMO polarized-antenna selection technique (AMPAS). The principle of this method is to choose properly the antenna polarizations that optimize the receiving signal power while minimizing fading correlation antenna effects. In Fig.1.19, an example of an adaptive polarization system employing 4 z-oriented dipoles at transmitter and 4 pairs of y- and z-oriented dipoles at receiver is illustrated. Simulation results based on 3D ray-tracing techniques show that the channel capacity obtained by an adaptive polarization increases 7%-13% in comparison to the single polarization channel capacity.

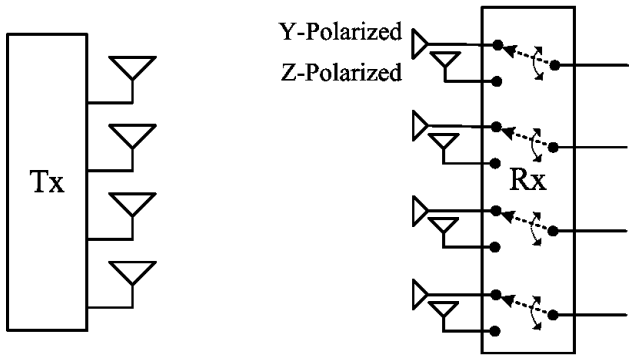

Figure 1.19: Adaptive polarization technique (AMPAS) at Rx

Another example of an adaptive polarization system is based on the rotation of the antenna elements according to the polarization of traveling waves at receiver. The proposed MIMO system consists of P half-wavelength dipole antennas that are rotated against one another by the rotation angle $\gamma = 180°/P$ with phase centers at the same point at both transmitter and receiver.

Fig.1.20 demonstrates the obtained performances of 1×1 SISO, 1×2 SIMO and 2×2 MIMO communication systems while the receiving antenna is rotating on y-z plane with χ_θ and $\chi_\phi \sim \mathcal{N}(0, 5)$. Performance can be better enhanced if polarization at the receiver is

properly matched to that of incident waves. In contrast, it can be worst if they are not well matched as shown in Fig.1.20a (at rotational angle (γ) $\approx 140°$). Thus for improving the MIMO channel capacity, the receiving antenna elements should be rotated to find maximum receiving signals while minimizing fading correlation antenna effects.

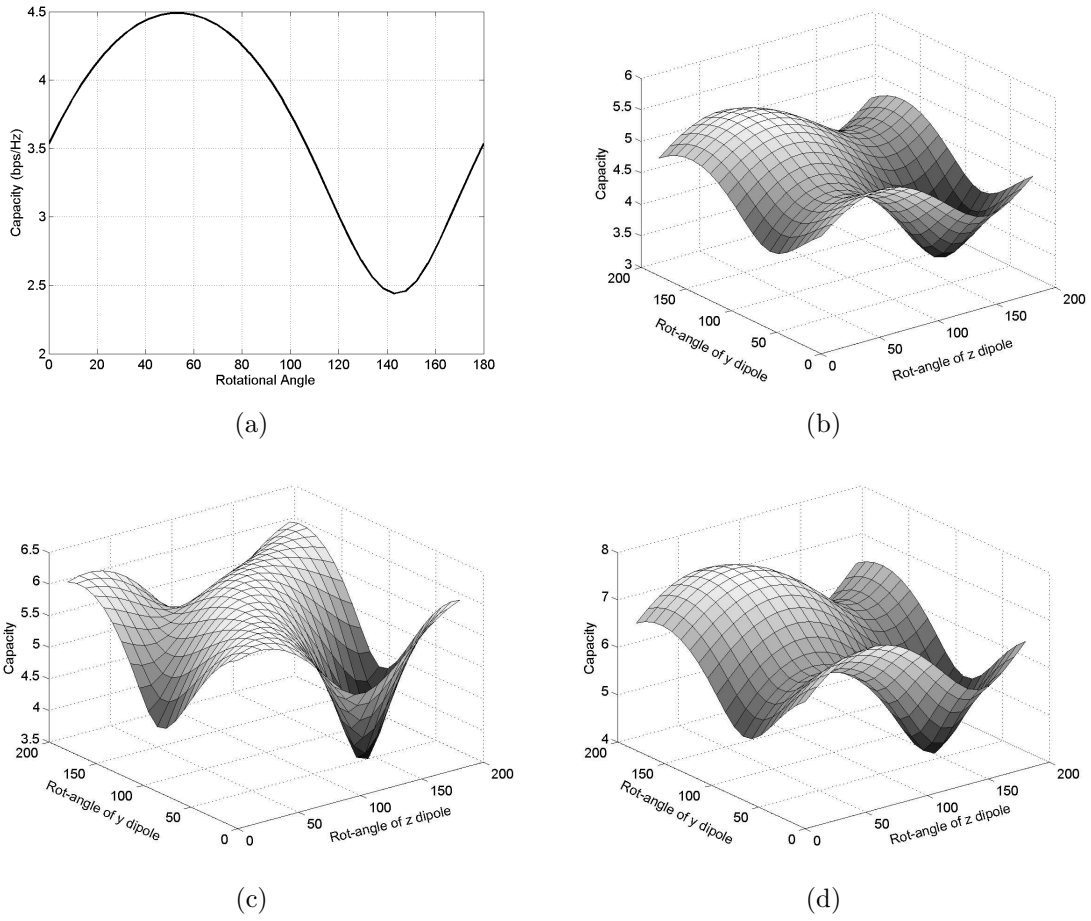

Figure 1.20: Performances of (a) 1×1 SISO, (b) 1×2 SIMO, (c) 2×2 MIMO as the same antenna position, (d) 2×2 MIMO as the separated antenna position while the receiving antenna is rotating on plane y-z

While the other systems employ only z-oriented dipoles at transmitter and y-, z-oriented dipoles at receiver in the case of the same antenna position (b,c) and the $\lambda/2$-separated antenna elements (d), the rotations of two dipoles on plane y-z can provide different performance as shown in Fig.1.20b,c and d. The channel performance is maximized performance in Fig.1.20b when the polarizations of receiving antennas are well matched and is minimized performance if they are mismatched. In Fig.1.20c, when the antennas have been rotated to

nearly the same position, high correlation is produced. Subsequently, the channel capacity is reduced even if the polarizations are correctly matched. However, it has better performance in the situation of polarization diversity when the antenna rotation has the difference of 90°. Moreover, we observe the MIMO capacity with spatial diversity as illustrated in Fig.1.20d where the antenna correlation is reduced and the channel capacity is improved.

In order to achieve a better transmission performance, the polarized antenna selection can exploit together all diversity techniques such as pattern, spatial and polarization diversity. Pattern diversity should be employed when a large angle spread is detected. Spatial diversity could be exploited when a high antenna correlation is observed. Polarization diversity should be used when a low XPD occurs. Therefore, the employed diversity should be properly selected according to the propagation environment.

1.6 MIMO applications

1.6.1 Wireless LAN based MIMO

In this chapter, it was shown that employing MIMO systems could achieve higher performance in data transmission. MIMO signalling can increase network bandwidth, range and reliability. Recently many communication systems begin to take advantage of this channel capacity enhancement such as Wireless Local Area Networks (WLAN) and Wireless Metropolitan Area Network (WMAN).

The IEEE 802.11 WLAN and the IEEE 802.16 WMAN standards are based on orthogonal frequency division multiplexing (OFDM). OFDM is a multi-carrier modulation system, reducing the required bandwidth but keeping the modulated signals orthogonal so they do not interfere with each other. An important high data transmission rate extension of these standards could be based on MIMO. An advantage of these systems is that they are principally deployed in indoor environments and suburban environments that are characterized by a rich multipath.

There are also some motivations in order to improve the performance and the transmission rate in MIMO-OFDM systems when the CSI is available at the transmitter. As mentioned in previous sections, water-filling technique is used to optimize the distribution of the total transmit power over transmit antennas. Therefore, information symbols and power could be optimally allocated over space and frequency in MIMO-OFDM communication.

The number of antennas utilized in a MIMO (WLAN) router for example can vary; typical MIMO router contains three or four antennas. These systems are driving the need for the next broadband revolution focused on home networking. Such systems will cover next-generation game consoles, Video-on-Demand, HDTV and other new products. These services are creating a more sophisticated home entertainment environment, together with a high level of Quality of Service (QoS) to facilitate multimedia connectivity.

The intelligence behind the antenna polarization is described as “adaptive polarization”.

The router receives feedback from the client adapter and has the ability to focus the polarization of the signals. As signal travels between an access point and wireless card, it will bounce off of walls, ceilings and any other obstacle, resulting in multiple reflections of the original signal arriving by different paths and different polarizations. By applying adaptive antenna polarization algorithms (AMPAS), these reflections can be used to improve the signal to noise ratio, as instead of having just one copy of the original signal.

This adaptive transmitting feature provides a more reliable signal at extreme ranges. Moreover, MIMO can eliminate dead spots, delivering reliable whole home coverage with all the speed you need for application in the future. Today, one can say, wireless is faster than leased wire systems.

Finally, MIMO networking has the potential to increase communications data rate by 10-20 times above current systems. Such systems will use multipath reflections to create parallel channels in the same frequency bandwidth, thereby increasing spectral efficiency.

In the next section sensor networks will be discussed as an application of MIMO based system.

1.6.2 MIMO for Cooperative Sensor Networks

A sensor network can be considered as a self contained circuit with its sensor and RF interface, as shown in Fig.1.21. Recent hardware advances allow more signal processing functionality to be integrated into a single chip. For example it is possible to integrate an RF transceiver, sensor interface, and base band processors into one device that is as small as a piece of coin and can be used as a fully-functional wireless sensor node. Such wireless nodes typically operate with small batteries, that is why these sensor nodes have limited power capabilities. In many scenarios, the wireless nodes must operate without battery replacement for many years. Consequently, minimizing the energy consumption is a very important design consideration and energy-efficient transmission schemes must be used for the data transfer in sensor networks

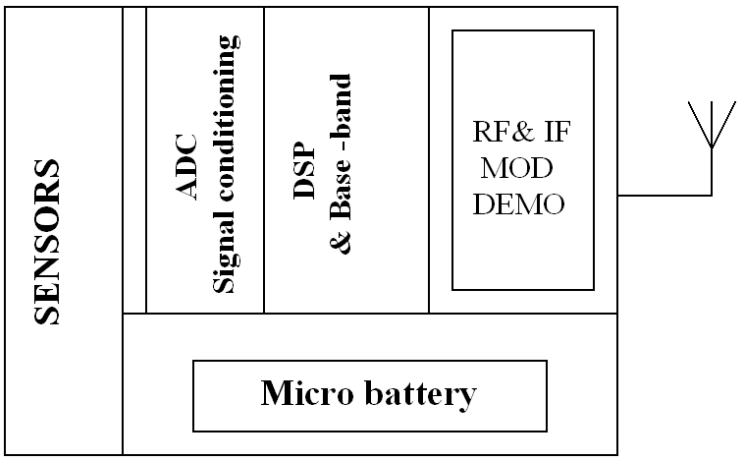

Figure 1.21: Typical wireless sensor node

In addition, because sensor nodes will be deployed in remote and oftentimes dangerous locations, their maintenance (in particular, battery replacement) will be unlikely [84].

Sensor Networks are a new attraction for many potential applications, such as industrial, military, geolocalization, surveillance, intrusion detection, and environmental monitoring [84], [85].

Robust communications between sensor nodes are highly demanded at low power. As it was shown, MIMO communication promises performance enhancements over conventional single-input single-output (SISO) technology without increasing the bandwidth consumed by the system or the total power radiated from a transmitter. MIMO technology has promising characteristics that make it a serious candidate for sensor network communication technology. Signal processing techniques that use multiple transmit and receive antennas, such as space-time coding (ST Coding), have been shown to increase transmission reliability.

In a surveillance application, the ability of sensor nodes to relay data is critical to the utility and effectiveness of the sensor network.

For a given node density, nodes are more likely to be out of range, thus inhibiting communication. In a situation such as this, the extended range of MIMO is of greater importance because it enables cohesion (the ability of the sensor nodes to form a completely connected network), which guarantees the success of the final application [86].

New protocols for target reporting and a procedure for target localization which conserve energy is recently developed [86],[87]. In [88], the authors summarize and compare several routing MIMO technology.

Mean path length provides a measurement of the impact of MIMO communications on a wireless sensor network. Mean path length provides a rough estimate of the amount of time and energy expended in a data transmission from one node to another in the network.

Most significant mean path length reduction is provided by MIMO in the low or midrange of node densities because the inter-node spacing is such that MIMO can reliably form some links that SISO cannot. In the elongated region scenario this trend holds, though it is less apparent [89].

There is also an increasing need for mobile networks with distributed transmitters and receivers, typically referred to as mobile ad hoc networks (MANET). There, transmitters and receivers do not pool their information together, either due to geographical dispersiveness, the bandwidth and resource limitation, or due to security/privacy concern.

Recognizing that multiple antennas at the transceivers provide inherent multiplexing capability due to their spatial selectivity, it is attractive to study MIMO communication in ad hoc networks with "interference" transmission.

Energy-efficient communication techniques typically focus on minimizing the transmission energy only, which is reasonable in long-range applications where the transmission energy is dominant in the total energy consumption.

In cooperative sensor networks, we allow the cooperation among sensors for information transmission and/or reception so as energy consumption as well as transmission delays over some distance ranges can be reduced.

In conclusion, for the same throughput requirement, MIMO systems require less transmission energy than SISO systems. However, direct application of multi-antenna techniques to sensor networks is impractical due to the limited physical size of a sensor node which typically can only support a single antenna. If individual single-antenna nodes allowed co-

operating on information transmission and/or reception, a cooperative MIMO system can be constructed such that energy-efficient MIMO schemes can be deployed [90].

Finally, MIMO can provide significant network performance improvements in power consumption, latency, and network robustness.

References

[1] E. Telatar, "Capacity of multi-antenna Gaussian channels," *European Trans. Telecommun.*, vol. 10, no. 6, pp. 585–595, Nov.-Dec. 1999.

[2] P. Bello, "Characterization of randomly time-variant linear channels," *IEEE Trans. Commun. Syst.*, vol. 11, pp. 360–393, 1963.

[3] J. Parsons, *The Mobile Radio Propagation Channel*. Wiley, 2000.

[4] G. Matz, "On non-WSSUS wireless fading channels," *IEEE Trans. Wireless Comm.*, vol. 4, no. 5, pp. 2465–2478, Sept. 2005.

[5] J. McJown and R. Hamilton, "Ray tracing as a design tool for radio networks," *IEEE Network Magazine*, pp. pp27–30, Nov. 1991.

[6] C. D. Kurner, T. and W. Wiesbeck, "Concepts and results for 3D digital terrain-based wave propagation models: An overview," *IEEE J. Sel. Areas Commun.*, vol. 11, pp. 1002–1012, 1993.

[7] R. Kouyoumjian and P. Pathak, "A uniform geometrical theory of diffraction for an edge in a perfectly conducting surface," *Proceedings of the IEEE*, vol. 62, no. 11, pp. 1448–1461, 1974.

[8] N. A. Athanasiadou, G.E and J. McGeehan, "A microcellular ray-tracing propagation model and evaluation of its narrowband and wideband," *IEEE J. Sel. Areas Commun.*, vol. 18, pp. 322–335, Mar 2000.

[9] R. J. Petrus, P. and T. Rappaport, "Geometrical-based statistical macrocell channel model for mobile environments," *IEEE Trans. Comm.*, vol. 50, no. 3, pp. 495–502, Mar. 2002.

[10] J. Liberti and T. Rappaport, "A geometrically based model for line-of-sight multipath radio channels," *in Proc. VTC*, pp. 844–848, Apr.-May 1996.

[11] E. V. Oestges, C. and A. Paulraj, "A physical scattering model for MIMO macrocellular broadband wireless channels," *IEEE J. Sel. Areas Commun.*, vol. 21, no. 5, pp. 721–729, June 2003.

[12] A. F. e. a. Molisch, "Geometry-based directional model for mobile radio channels - principles and implementation," *European Trans. Telecomm.*, vol. 14, pp. 351–359, 2003.

[13] K. Raoof and N. Prayongpun, "Channel capacity performance for MIMO polarized diversity systems," *in Proc. WCNM*, pp. 1–4, Sep 2005.

[14] G. J. Foschini and M. J. Gans, "On limits of wireless communications in a fading environment when using multiple antennas," *Wireless Personal Commun.*, vol. 6, no. 3, pp. 311–335, Mar. 1998.

[15] M. A. Khalighi, K. Raoof, and G. Jourdain, "Capacity of wireless communication systems employing antenna arrays, a tutorial study," *Wireless Personal Commun.*, vol. 23, no. 3, pp. 321–352, Dec. 2002.

[16] D. Shiu, G. J. Foschini, M. J. Gans, and J. M. Kahn, "Fading correlation and its effect on the capacity of multi-element antenna systems," *IEEE Trans. Commun.*, vol. 48, no. 3, pp. 502–513, Mar. 2000.

[17] J. e. a. Kermoal, "A stochastic MIMO radio channel model with experimental validation," *IEEE J. Sel. Areas Commun.*, vol. 20, no. 6, pp. 1211–1226, 2002.

[18] H. a. zcelik, "Deficiencies of the 'kronecker' MIMO radio channel model," *in Proc. WPMC*, Oct. 2003.

[19] A. Saleh and R. Valenzuela, "A statistical model for indoor multipath propagation," *IEEE J. Sel. Areas Commun.*, vol. 5, no. 2, pp. 128–137, Feb. 1987.

[20] D. e. a. Gesbert, "Outdoor MIMO wireless channels: Models and performance prediction," *IEEE Trans. Commun.*, vol. 50, pp. 1926–1934, Dec. 2002.

[21] A. Burr, "Capacity bounds and estimates for the finite scatterers MIMO wireless channel," *IEEE J. Sel. Aseas Comm.*, vol. 21, no. 5, pp. 812–818, June 2003.

[22] M. Debbah and R. Muller, "MIMO channel modeling and the principle of maximum

entropy," *IEEE Trans. Inf. Theory*, vol. 51, no. 5, May 2005.
[23] A. Sayeed, "Deconstructing multiantenna fading channels," *IEEE Trans. Signal Processing*, vol. 50, no. 10, pp. 2563–2579, Oct 2002.
[24] L. Correia, *Wireless Flexible Personalised Communication* (COST 259 Final Report). Wiley, 2001.
[25] ——, *Mobile Broadband Multimedia Networks* (COST 273 Final Report). Elsevier, 2006.
[26] 3GPP-3GPP2 TR 25.996, "Spatial channel model for multiple input multiple output (MIMO) simulations," (2003-09).
[27] G. J. Foschini, "Layered space-time architecture for wireless communication in a fading environment when using multi-element antennas," *Bell Labs Tech. J.*, vol. 1, no. 2, pp. 41–59, Autumn 1996.
[28] G. D. Golden, G. J. Foschini, R. A. Valenzuela, and P. W. Wolniansky, "Detection algorithm and initial laboratory results using V-BLAST space-time communication architecture," *Electronic Lett.*, vol. 35, no. 1, pp. 14–16, Jan. 1999.
[29] G. G. Raleigh and V. K. Jones, "Multivariate modulation and coding for wireless communication," *IEEE J. Sel. Areas Commun.*, vol. 17, no. 5, pp. 851–866, May 1999.
[30] E. Biglieri, J. Proakis, and S. S. (Shitz), "Fading channels, information-theoretic and communications aspects," *IEEE Trans. Inf. Theory*, vol. 44, no. 6, pp. 2619–2692, Oct. 1998.
[31] W. C. Jakes, *Microwave Mobile Communications*. New York: John Wiley & Sons, 1974, reprinted by IEEE Press, 1998.
[32] H. Hashemi, "The indoor radio propagation channel," *Proceedings of the IEEE*, vol. 81, no. 7, pp. 943–968, July 1993.
[33] M. A. Khalighi, J. M. Brossier, G. Jourdain, and K. Raoof, "Water filling capacity of Rayleigh MIMO channels," *in Proc. PIMRC*, vol. A, pp. 155–158, Sept.-Oct. 2001, San Diego, CA.
[34] J. B. Anderson, "Array gain and capacity for known random channels with multiple element arrays at both ends," *IEEE J. Sel. Areas Commun.*, vol. 18, no. 11, pp. 2172–2178, Nov. 2000.
[35] G. G. Raleigh and J. M. Cioffi, "Spatio-temporal coding for wireless communication," *IEEE Trans. Commun.*, vol. 46, no. 3, pp. 357–366, Mar. 1998.
[36] T. L. Marzetta and B. M. Hochwald, "Capacity of a mobile multiple-antenna communication link in Rayleigh flat fading," *IEEE Trans. Inf. Theory*, vol. 45, no. 1, pp. 139–157, Jan. 1999.
[37] L. Zheng and D. N. C. Tse, "Communication on the Grassmann Manifold: a geometric approach to the noncoherent multiple-antenna channel," *IEEE Trans. Inf. Theory*, vol. 48, no. 2, pp. 359–383, Feb. 2002.
[38] B. Sklar, "Rayleigh fading channels in mobile digital communication systems; Part I: Characterization; Part II: Mitigation," *IEEE Commun. Mag.*, vol. 35, no. 7, pp. 90–109, Oct. 1997.
[39] J. Salz and J. H. Winters, "Effect of fading correlation on adaptive arrays in digital mobile radio," *IEEE Trans. Veh. Technol.*, vol. 43, no. 4, pp. 1049–1057, Nov. 1994.
[40] P. F. Driessen and G. J. Foschini, "On the capacity formula for multiple input-multiple output wireless channels: a geometric interpretation," *IEEE Trans. Commun.*, vol. 47, no. 2, pp. 173–176, Feb. 1999.
[41] M. A. Khalighi, J. M. Brossier, G. Jourdain, and K. Raoof, "On capacity of Ricean MIMO channels," *in Proc. PIMRC*, vol. A, pp. 150–154, Sept.-Oct. 2001, San Diego, CA.
[42] C. Berrou and A. Glavieux, "Near optimum error correcting coding and decoding: turbo-codes," *IEEE Trans. Commun.*, vol. 44, no. 10, pp. 1261–1271, Oct. 1996.
[43] C. Douillard, M. Jézéquel, C. Berrou, A. Picart, P. Didier, and A. Glavieux, "Iterative

correction of intersymbol interference: Turbo-equalization," *European Trans. Telecommun.*, vol. 6, no. 5, pp. 507–511, Sept.-Oct. 1995.
[44] M. A. Khalighi and J. J. Boutros, "Semi-blind channel estimation using EM algorithm in iterative MIMO APP detectors," *IEEE Trans. Wireless Commun.*, vol. 5, no. 11, pp. 3165–3173, Nov. 2006.
[45] N. Noels, C. Herzet, A. Dejonghe, V. Lottici, H. Steendam, M. Moeneclaey, M. Luise, and L. Vandendorpe, "Turbo synchronization: An EM algorithm interpretation," *in Proc. ICC*, vol. 4, pp. 2933–2937, May 2003, Anchorage, AK.
[46] H. El Gamal and E. Geraniotis, "Iterative multiuser detection for coded CDMA signals in AWGN and fading channels," *IEEE J. Sel. Areas Commun.*, vol. 18, no. 1, pp. 30–41, Jan. 2000.
[47] M. Sellathurai and S. Haykin, "Turbo-BLAST for wireless communications: theory and experiments," *IEEE Trans. Signal Processing*, vol. 50, no. 10, pp. 2538– 2546, Oct. 2002.
[48] B. Vucetic and J. Yuan, *Space-Time Coding.* Chichester, England: John Wiley & Sons Ltd, 2003.
[49] V. Tarokh, H. Jafarkhani, and A. Calderbank, "Space-time block codes from orthogonal designs," *IEEE Trans. Inf. Theory*, vol. 45, no. 5, pp. 1456–1467, July 1999.
[50] S. Alamouti, "A simple transmit diversity technique for wireless communications," *IEEE J. Sel. Areas Commun.*, vol. 16, no. 8, pp. 1451–1458, Oct. 1998.
[51] V. Tarokh, N. Seshadri, and A. R. Calderbank, "Space-time codes for high data rate wireless communication: performance criterion and code construction," *IEEE Trans. Inf. Theory*, vol. 44, no. 2, pp. 744–765, Mar. 1998.
[52] Y. Xin, Z. Wang, and G. B. Giannakis, "Space-time diversity systems based on linear constellation precoding," *IEEE Trans. Wireless Commun.*, vol. 2, no. 3, pp. 294–309, Mar. 2003.
[53] B. Hassibi and B. Hochwald, "High-rate codes that are linear in space and time," *IEEE Trans. Inf. Theory*, vol. 48, no. 7, pp. 1804–1824, July 2002.
[54] E. Viterbo and J. Boutros, "A universal lattice code decoder for fading channels," *IEEE Trans. Inf. Theory*, vol. 45, no. 5, pp. 1639–1642, July 1999.
[55] G. Caire, G. Taricco, and E. Biglieri, "Bit-interleaved coded modulation," *IEEE Trans. Inf. Theory*, vol. 44, no. 3, pp. 927–946, May 1998.
[56] L. Bahl, J. Cocke, F. Jelinek, and J. Raviv, "Optimal decoding of linear codes for minimizing symbol error rate," *IEEE Trans. Inf. Theory*, vol. 20, no. 2, pp. 284–287, Mar. 1974.
[57] J. Hagenauer, E. Offer, and L. Papke, "Iterative decoding of binary block and convolutional codes," *IEEE Trans. Inf. Theory*, vol. 42, no. 2, pp. 429–445, Mar. 1996.
[58] P. Robertson, P. Hoeher, and E. Villebrun, "Optimal and sub-optimal maximum a posteriori algorithms suitable for turbo decoding," *European Trans. Telecommun.*, vol. 8, no. 2, pp. 119–125, Mar.-Apr. 1997.
[59] J. Boutros, N. Gresset, and L. Brunel, "Turbo coding and decoding for multiple antenna channels," *in Proc. Int. Symp. on Turbo Codes and Related Topics*, Sept. 2003, Brest, France.
[60] B. Hassibi and H. Vikalo, "On the sphere-decoding algorithm I. Expected complexity," *IEEE Trans. Signal Processing*, vol. 53, no. 8, pp. 2806–2818, Aug. 2005.
[61] M. Khalighi and J. Boutros, "Channel estimation in turbo-BLAST detectors using EM algorithm," *in Proc. ICASSP*, vol. III, pp. 1037–1040, Mar. 2005, Philadelphia, PA.
[62] M. A. Khalighi, J. Boutros, and J.-F. Hélard, "Data-aided channel estimation for Turbo-PIC MIMO detectors," *IEEE Commun. Lett.*, vol. 10, no. 5, pp. 350–352, May 2006.
[63] M. A. Khalighi and J.-F. Hélard, "Should MIMO orthogonal space-time coding be preferred to non-orthogonal coding with iterative detection?" *in Proc. ISSPIT*, pp. 340–345, Dec. 2005, Athens, Greece.
[64] X. Wang and H. V. Poor, "Iterative (turbo) soft interference cancellation and deoding

for coded CDMA," *IEEE Trans. Commun.*, vol. 47, no. 7, pp. 1046–1061, July 1999.
[65] M. A. Khalighi, J.-F. Hélard, and S. Bourennane, "Choice of appropriate space-time coding scheme for MIMO systems employing channel coding under BICM," *In Proc. SPAWC*, July 2006, Cannes, France.
[66] ——, "Contrasting orthogonal and non-orthogonal space-time schemes for perfectly-known and estimated MIMO channels," *in Proc. ICCS*, Oct.-Nov. 2006, Singapore.
[67] V. Le Nir, J.-M. Auffray, M. Hélard, J.-F. Hélard, and R. Le Gouable, "Combination of space-time block coding with MC-CDMA technique for MIMO systems with two, three and four transmit antennas," *in Proc. IST Mobile Commun. Summit Conf.*, June 2003, Aveiro, Portugal.
[68] J.-C. Belfiore, G. Rekaya, and E. Viterbo, "The golden code: a 2×2 full-rate space-time code with nonvanishing determinants," *IEEE Trans. Inf. Theory*, vol. 51, no. 4, pp. 1432–1436, Apr. 2005.
[69] R. Vaughan, "Beam spacing for angle diversity," *in Proc. Globecom*, vol. 2, pp. 928 – 933, Nov 1998.
[70] P. e. a. Kyritsi, "Effect of antenna polarization on the capacity of a multiple element system in an indoor environment," *IEEE J. Sel. Areas Commun.*, vol. 20, pp. 1227–1239, Aug . 2002.
[71] S. H. Eiceg, V. and Catreux, "Dual-polarization versus single-polarization MIMO channel measurement results and modeling," *IEEE Trans. Wireless Commun.*, vol. 5, no. 28- 33, Jan. 2006.
[72] T. Svantesson., "On the potential of multimode antenna diversity," *in Proc. VTC*, Sep. 2000.
[73] J. M. Svantesson, T. and J. Wallace, "Analysis of electromagnetic field polarizations in multiantenna systems," *IEEE Trans. Wireless Commun.*, vol. 3, pp. 641– 646, March 2004.
[74] J. Andersen and B. Getu, "The mimo cube - a compact MIMO antenna," *Wireless Personal Multimedia Commun.*, vol. 1, pp. 112– 114, Oct. 2002.
[75] C. A. Balanis, *Antenna Theory*. New York: John Wiley and Sons, 1997.
[76] V. E. R. K. P. Soma, D.S. Baum1 and A. Paulraj, "Analysis and modeling of multiple-input multiple-output (MIMO) radio channel based on outdoor measurements conducted at 2.5GHz for fixed BWA applications," *in Proc. ICC*, pp. 272 – 276, April 2002.
[77] R. Vaughan, "Polarization diversity in mobile communications," *IEEE Trans. Veh. Technol.*, vol. 39, no. 3, August 1990.
[78] A. W. J. Lempiainen, J.K. Laiho-Steffens, "Experimental results of cross polarization discrimination andsignal correlation values for a polarization diversity scheme," *in Proc VTC*, pp. 1498 – 1502, May 1997.
[79] T. Svantesson, "Correlation and channel capacity of MIMO systems employing multimode antennas," *IEEE Trans. Veh. Technol.*, vol. 51, no. 6, Nov. 2002.
[80] A. F. Molisch, "A generic model for the MIMO wireless propagation channels in macro- and microcells," *IEEE Trans. Signal Processing*, vol. 52, no. 1, pp. 61–71, Jan. 2004.
[81] S. Yong and J. Thompson, "A three-dimensional spatial fading correlation model for uniform rectangular arrays," *IEEE Antennas Wireless Propagat. Lett.*, vol. 2, 2003.
[82] P. M. M.R. Andrews and R. deCarvalho, "Tripling the capacity of wireless communication using electromagnetic polarization," *Nature*, vol. 409, pp. 316–318, Jan. 2001.
[83] N. Prayongpun and K. Raoof, "MIMO channel capacities in presence of polarization diversity with and without line-of-sight path," *Journal WSEAS Trans. Commun.*, vol. 5, no. 9, pp. 1744–1750, Sep. 2006.
[84] I. A. et al., "A survey on sensor networks," *IEEE Commun. Mag.*, pp. 102–114, Aug 2002.
[85] C. Chong and S. Kumar, "Sensor networks: Evolution, opportunities, and challenges,"

Proceedings of the IEEE, vol. 91, no. 8, pp. 1247–1256, Aug. 2003.
[86] J. Burdin and J. Dunyak, "Cohesion of wireless sensor networks with MIMO communications," MITRE Corp., Tech. Rep., Sep. 2006.
[87] J. L. L. Godard and K. Raoof, "Localisation des objets communicants," Laboratoire LIS, Tech. Rep., Sep. 2006.
[88] Q. Jiang and D. Manivarman, "Routing protocols for sensor networks," *Consumer Communications and Networking Conference*, pp. 93–98, Jan. 2004.
[89] J. Burdin and J. Dunyak, "Enhancing the performance of wireless sensor networks with MIMO communications," MITRE Corp., Tech. Rep., Sep. 2006.
[90] A. J. G. S. Cui and A. Bahai, "Energy-efficiency of MIMO and cooperative MIMO techniques in sensor networks," *IEEE J. Sel. Areas Commun.*, 2004.

List of Figures